Analysis Procedures for Evaluating Superheavy Load Movement on Flexible Pavements, Volume V: Appendix D, Estimation of Subgrade Shear Strength Parameters Using Falling Weight Deflectometer

PUBLICATION NO. FHWA-HRT-18-053

JANUARY 2019

U.S. Department of Transportation
Federal Highway Administration

Research, Development, and Technology
Turner-Fairbank Highway Research Center
6300 Georgetown Pike
McLean, VA 22101-2296

FOREWORD

The movement of superheavy loads (SHLs) on the Nation's highways is an increasingly common, vital economic necessity for many important industries, such as chemical, oil, electrical, and defense. Many superheavy components are extremely large and heavy (gross vehicle weights in excess of a few million pounds), and they often require specialized trailers and hauling units. At times, SHL vehicles have been assembled to suit the load being transported, and therefore, the axle configurations have not been standard or consistent. Accommodating SHL movements without undue damage to highway infrastructure requires the determination of whether the pavement is structurally adequate to sustain the SHL movement and protect any underground utilities. Such determination involves analyzing the likelihood of instantaneous or rapid load-induced shear failure of the pavement structure.

The goal of this project was to develop a comprehensive analysis process for evaluating SHL movement on flexible pavements. As part of this project, a comprehensive mechanistic-based analysis approach consisting of several analysis procedures was developed for flexible pavement structures and documented in a 10-volume series of Federal Highway Administration reports—a final report and 9 appendices.[1–9] This is *Analysis Procedures for Evaluating Superheavy Load Movement on Flexible Pavements, Volume V: Appendix D, Estimation of Subgrade Shear Strength Parameters Using Falling Weight Deflectometer*, and it presents an approach to estimate the shear strength parameters of a pavement's subgrade layer based on nondestructive falling weight deflectometer measurements. This report is intended for use by highway agency pavement engineers responsible for assessing the structural adequacy of pavements in the proposed route and identifying mitigation strategies, where warranted, in support of the agency's response to SHL-movement permit requests.

Cheryl Allen Richter, Ph.D., P.E.
Director, Office of Infrastructure
Research and Development

TECHNICAL REPORT DOCUMENTATION PAGE

1. Report No. FHWA-HRT-18-053	2. Government Accession No.	3. Recipient's Catalog No.
4. Title and Subtitle Analysis Procedures for Evaluating Superheavy Load Movement on Flexible Pavements, Volume V: Appendix D, Estimation of Subgrade Shear Strength Parameters Using Falling Weight Deflectometer		5. Report Date January 2019 6. Performing Organization Code
7. Author(s) Hadi Nabizadeh (ORCID: 0000-0001-8215-1299), Elie Y. Hajj (ORCID: 0000-0001-8568-6360), Raj V. Siddharthan (ORCID: 0000-0002-3847-7934), Mohamed Nimeri (ORCID: 0000-0002-3328-4367), Sherif Elfass (ORCID: 0000-0003-3401-6513), and Murugaiyah Piratheepan (ORCID: 0000-0002-3302-4856)		8. Performing Organization Report No. WRSC-UNR-201710-01D
9. Performing Organization Name and Address Department of Civil and Environmental Engineering University of Nevada 1664 North Virginia Street Reno, NV 89557		10. Work Unit No. 11. Contract or Grant No. DTFH61-13-C-00014
12. Sponsoring Agency Name and Address Office of Infrastructure Research and Development Federal Highway Administration Turner-Fairbank Highway Research Center 6300 Georgetown Pike McLean, VA 22101		13. Type of Report and Period Covered Final Report; August 2013–July 2018 14. Sponsoring Agency Code HRDI-20
15. Supplementary Notes Nadarajah Sivaneswaran (HRDI-20; ORCID: 0000-0003-0287-664X), Office of Infrastructure Research and Development, Turner-Fairbank Highway Research Center, served as the Contracting Officer's Representative.		
16. Abstract The movement of superheavy loads (SHLs) has become more common over the years since it is a vital necessity for many important industries, such as chemical, oil, electrical, and defense. SHL hauling units are much larger in size and weight compared to standard trucks. SHL gross vehicle weights may be in excess of a few million pounds, so they often require specialized trailers and components with nonstandard spacing between tires and axles. Accommodating SHL movements requires the determination of whether a pavement is structurally adequate and involves the analysis of the likelihood of instantaneous or rapid load-induced shear failure. As part of the Federal Highway Administration project, Analysis Procedures for Evaluating Superheavy Load Movement on Flexible Pavements, a novel methodology to estimate in-situ shear strength parameters (angle of internal friction (ϕ) and cohesion (c)) of a pavement's subgrade (SG) layer was developed and verified. The approach is based on nondestructive falling weight deflectometer (FWD) testing undertaken at multiple load levels. The validity of the proposed approach was explored using numerical simulations of FWD tests, as well as FWD data collected from large-scale experiments on full-scale pavement structures and Accelerated Pavement Testing facilities. It was found that the proposed FWD-based methodology was able to reasonably estimate ϕ and c of an SG layer with softening behavior. Such results were achieved when the highest induced deviator stress level in the SG layer under the FWD loading was in excess of approximately 30 percent of the deviator stress at failure obtained with the proposed procedure.		
17. Key Words Flexible pavement, superheavy load, large-scale experiment, FWD, LWD, shear strength	18. Distribution Statement No restrictions. This document is available to the public through the National Technical Information Service, Springfield, VA 22161. http://www.ntis.gov	

19. Security Classif. (of this report) Unclassified	20. Security Classif. (of this page) Unclassified	21. No. of Pages 47	22. Price N/A

Form DOT F 1700.7 (8-72) Reproduction of completed page authorized.

SI* (MODERN METRIC) CONVERSION FACTORS

APPROXIMATE CONVERSIONS TO SI UNITS

Symbol	When You Know	Multiply By	To Find	Symbol
		LENGTH		
in	inches	25.4	millimeters	mm
ft	feet	0.305	meters	m
yd	yards	0.914	meters	m
mi	miles	1.61	kilometers	km
		AREA		
in^2	square inches	645.2	square millimeters	mm^2
ft^2	square feet	0.093	square meters	m^2
yd^2	square yard	0.836	square meters	m^2
ac	acres	0.405	hectares	ha
mi^2	square miles	2.59	square kilometers	km^2
		VOLUME		
fl oz	fluid ounces	29.57	milliliters	mL
gal	gallons	3.785	liters	L
ft^3	cubic feet	0.028	cubic meters	m^3
yd^3	cubic yards	0.765	cubic meters	m^3
		NOTE: volumes greater than 1000 L shall be shown in m^3		
		MASS		
oz	ounces	28.35	grams	g
lb	pounds	0.454	kilograms	kg
T	short tons (2000 lb)	0.907	megagrams (or "metric ton")	Mg (or "t")
		TEMPERATURE (exact degrees)		
^oF	Fahrenheit	5 (F-32)/9 or (F-32)/1.8	Celsius	^oC
		ILLUMINATION		
fc	foot-candles	10.76	lux	lx
fl	foot-Lamberts	3.426	$candela/m^2$	cd/m^2
		FORCE and PRESSURE or STRESS		
lbf	poundforce	4.45	newtons	N
lbf/in^2	poundforce per square inch	6.89	kilopascals	kPa

APPROXIMATE CONVERSIONS FROM SI UNITS

Symbol	When You Know	Multiply By	To Find	Symbol
		LENGTH		
mm	millimeters	0.039	inches	in
m	meters	3.28	feet	ft
m	meters	1.09	yards	yd
km	kilometers	0.621	miles	mi
		AREA		
mm^2	square millimeters	0.0016	square inches	in^2
m^2	square meters	10.764	square feet	ft^2
m^2	square meters	1.195	square yards	yd^2
ha	hectares	2.47	acres	ac
km^2	square kilometers	0.386	square miles	mi^2
		VOLUME		
mL	milliliters	0.034	fluid ounces	fl oz
L	liters	0.264	gallons	gal
m^3	cubic meters	35.314	cubic feet	ft^3
m^3	cubic meters	1.307	cubic yards	yd^3
		MASS		
g	grams	0.035	ounces	oz
kg	kilograms	2.202	pounds	lb
Mg (or "t")	megagrams (or "metric ton")	1.103	short tons (2000 lb)	T
		TEMPERATURE (exact degrees)		
^oC	Celsius	1.8C+32	Fahrenheit	^oF
		ILLUMINATION		
lx	lux	0.0929	foot-candles	fc
cd/m^2	$candela/m^2$	0.2919	foot-Lamberts	fl
		FORCE and PRESSURE or STRESS		
N	newtons	0.225	poundforce	lbf
kPa	kilopascals	0.145	poundforce per square inch	lbf/in^2

ANALYSIS PROCEDURES FOR EVALUATING SUPERHEAVY LOAD MOVEMENT ON FLEXIBLE PAVEMENTS PROJECT REPORT SERIES

This volume is the fifth of 10 volumes in this research report series. Volume I is the final report, and Volume II though Volume X consist of Appendix A through Appendix I. Any reference to a report volume in this series will be referenced in the text as "Volume I: Appendix A," "Volume II: Appendix B," and so forth. The following list contains the volumes:

Volume	Title	Report Number
I	Analysis Procedures for Evaluating Superheavy Load Movement on Flexible Pavements, Volume I: Final Report	FHWA-HRT-18-049
II	Analysis Procedures for Evaluating Superheavy Load Movement on Flexible Pavements, Volume II: Appendix A, Experimental Program	FHWA-HRT-18-050
III	Analysis Procedures for Evaluating Superheavy Load Movement on Flexible Pavements, Volume III: Appendix B, Superheavy Load Configurations and Nucleus of Analysis Vehicle	FHWA-HRT-18-051
IV	Analysis Procedures for Evaluating Superheavy Load Movement on Flexible Pavements, Volume IV: Appendix C, Material Characterization for Superheavy Load Movement Analysis	FHWA-HRT-18-052
V	Analysis Procedures for Evaluating Superheavy Load Movement on Flexible Pavements, Volume V: Appendix D, Estimation of Subgrade Shear Strength Parameters Using Falling Weight Deflectometer	FHWA-HRT-18-053
VI	Analysis Procedures for Evaluating Superheavy Load Movement on Flexible Pavements, Volume VI: Appendix E, Ultimate and Service Limit Analyses	FHWA-HRT-18-054
VII	Analysis Procedures for Evaluating Superheavy Load Movement on Flexible Pavements, Volume VII: Appendix F, Failure Analysis of Sloped Pavement Shoulders	FHWA-HRT-18-055
VIII	Analysis Procedures for Evaluating Superheavy Load Movement on Flexible Pavements, Volume VIII: Appendix G, Risk Analysis of Buried Utilities Under Superheavy Load Vehicle Movements	FHWA-HRT-18-056
IX	Analysis Procedures for Evaluating Superheavy Load Movement on Flexible Pavements, Volume IX: Appendix H, Analysis of Cost Allocation Associated With Pavement Damage Under a Superheavy Load Vehicle Movement	FHWA-HRT-18-057
X	Analysis Procedures for Evaluating Superheavy Load Movement on Flexible Pavements, Volume X: Appendix I, Analysis Package for Superheavy Load Vehicle Movement on Flexible Pavement (SuperPACK)	FHWA-HRT-18-058

TABLE OF CONTENTS

LIST OF FIGURES

LIST OF TABLES

LIST OF ABBREVIATIONS AND SYMBOLS

Abbreviations

3D	three-dimensional
AC	asphalt concrete
APT	Accelerated Pavement Testing
CAB	crushed aggregate base
DR	deflection ratio
FAA	Federal Aviation Administration
FWD	falling weight deflectometer
LEP	linear elastic program
LVDT	linear variable differential transformer
LWD	light weight deflectometer
NAPTF	National Airport Pavement Test Facility
RMSE	root-mean-square error
SC	clayey sand with gravel
SG	subgrade
SHL	superheavy load

Symbols

B_{FWD}	FWD-plate diameter
c	cohesion
E_i	initial tangent modulus
E_{Ri}	breakpoint resilient modulus
K	regression constant of resilient modulus model
K_0	lateral earth pressure coefficient
K_3	slope of linear in bilinear model before breakpoint deviator stress
K_4	slope of linear in bilinear model after breakpoint deviator stress
m	deviator stress exponent
M_R	resilient modulus
$(M_R)_{SG}$	backcalculated subgrade resilient modulus
n	bulk stress exponent
P_{max}	maximum contact pressure
r	plate radius
v	Poisson's ratio
δ_c	maximum surface deflection at the center
ε_1	axial strain
θ	bulk stress
σ_1	major principal stress
σ_2	intermediate principal stress
σ_3	minor principal stress
σ_c	confining stress
$\sigma_{c\text{-}avg}$	average of confining stresses
σ_d	deviator stress

σ_{df}	deviator stress at failure
σ_{di}	breakpoint deviator stress
σ_{dll}	deviator stress lower limit
σ_{dul}	deviator stress upper limit
σ_{ij}	stress tensor
σ_{oct}	octahedral normal stress
σ_{v}	vertical stress
τ_{oct}	octahedral shear stress
ϕ	angle of internal friction

CHAPTER 1. INTRODUCTION

As previously elaborated in Volume III: Appendix B, superheavy load (SHL) components are much larger in size and weight than standard trucks, and they often require specialized trailers and hauling units.[3] The weights of these SHLs sometimes approach 6 million lb. The axle and tire configurations to be used are variable as they are often assembled to suit the specific superheavy components being transported. This variability leads to spacing between tires and axles that is not standard, and the tire imprints, as a whole, can span multiple lanes.

The vertical-stress (σ_v) distribution below the pavement surface under an SHL vehicle can be important because overlapping stress distributions under the tire loads can render a critical condition of instantaneous failure or onset of yielding, especially in the subgrade (SG). Though the SG thickness can be substantially large in many field situations, the area of interest is the SG zone that is affected by the truck surface load. This zone is the most vulnerable location to failure under an SHL vehicle movement and needs to be characterized to estimate pavement performance. In this report, the term pavement SG layer refers to this zone.

The SG layer's shear strength parameters (angle of internal friction (ϕ) and cohesion (c)) are necessary inputs for investigating the bearing capacity (i.e., instantaneous) failure and the onset of yielding of the SG layer under the SHL configuration. The shear strength parameters are not readily available and are not used in routine pavement-design processes. Many researchers have cautioned against using the existing database of ϕ and c values to characterize the strength of a pavement SG layer, which is mainly because of the variable nature of the SG layer. Direct estimation of ϕ and c values under in-situ conditions for pavement SG layer is often recommended. Although laboratory testing provides the most reliable measurements for shear strength parameters of unbound materials (e.g., base and SG), its practical limitations include the time-consuming and destructive processes of sample collecting, testing, and associated costs. On the other hand, use of engineering judgment can lead to an inaccurate determination of in-situ shear strength parameters.

As part of the Federal Highway Administration project, Analysis Procedures for Evaluating Superheavy Load Movement on Flexible Pavements, a comprehensive mechanistic-based analysis approach consisting of several analysis procedures was developed. A summary of the various analysis procedures developed in this study and associated objectives (including related volume numbers) are summarized in table 1. This report is the fifth of 10 volumes and presents a novel methodology to estimate in-situ shear strength parameters (ϕ and c) of pavement SG layers.[1–9]

Falling weight deflectometers (FWDs) are among the most acclaimed nondestructive testing devices that simulate pavement responses under the wheel of a moving truck. A stationary impact load of known magnitude is applied to the asphalt pavement surface. The applied load, in conjunction with the measured vertical surface displacements at different radial distances, commonly termed as deflection basins, is routinely utilized to estimate resilient moduli (M_R) of the various pavement layers using computational backcalculation techniques. Estimated layer stiffnesses derived using such procedures are implemented in investigation of the structural adequacy of pavement structures.

Table 1. Developed analysis procedures to evaluate SHL movements on flexible pavements.

Procedure	Objective
SHL analysis vehicle	Identify segment(s) of the SHL-vehicle configuration that can be regarded as representative of the entire SHL vehicle (Volume III: Appendix B)[3]
Flexible pavement structure	Characterize representative material properties for existing pavement layers (Volume IV: Appendix C and Volume V: Appendix D)[4]
SG bearing failure analysis	Investigate instantaneous ultimate shear failure in pavement SG (Volume VI: Appendix E)[5]
Sloped-shoulder failure analysis	Examine the stability of sloped pavement shoulder under an SHL-vehicle movement (Volume VII: Appendix F)[6]
Buried utility risk analysis	Perform risk analysis of existing buried utilities (Volume VIII: Appendix G)[7]
Localized shear failure analysis	Inspect the likelihood of localized failure (yield) in the pavement SG (Volume VI: Appendix E)[5]
Deflection-based service limit analysis	Investigate the development of premature surface distresses (Volume VI: Appendix E)[5]
Cost allocation analysis	Determine pavement damage–associated cost attributable to SHL-vehicle movement (Volume IX: Appendix H)[8]

Despite the fact that FWD devices have been successfully employed to estimate pavement-layer stiffness and pavement-structure load-carrying capacity, the applicability of these devices to determine the in-situ shear strength parameters of pavement layers has not been examined by researchers. A novel FWD-based methodology for estimating in-situ ϕ and c of the pavement SG layer, which contributes to pavement performance, has been developed as a part of this study. The methodology includes consideration of the stress-dependent behavior of the SG material assessed based on the backcalculation process using deflection basins from different FWD load levels.

In this report, the feasibility of using FWD measurements to estimate the strength parameters of an SG layer is demonstrated. The validity of the proposed approach was explored using numerical simulations of FWD tests, as well as FWD data collected from large-scale experiments on full-scale pavement structures and Accelerated Pavement Testing (APT) facilities. A variety of unpaved and paved pavement structures were utilized in the verification process.

CHAPTER 2. METHODOLOGY

In this chapter, the FWD-based methodology for estimating in-situ total shear strength parameters (ϕ and c) of an SG layer is described.

2.1. NONLINEAR HYPERBOLIC STRESS–STRAIN RELATIONSHIP OF SOILS

The laboratory triaxial compression tests have been traditionally used to determine the shear strength parameters of soils. A typical stress–strain relationship in the triaxial compression test is often expressed by a hyperbola as presented in figure 1.[10,11]

$$\sigma_d = \frac{\varepsilon_1}{\frac{1}{E_i} + \frac{\varepsilon_1}{\sigma_{df}}}$$

Figure 1. Equation. Nonlinear hyperbolic stress–strain relationship of soils.

Where:

σ_d = deviator stress.
ε_1 = axial strain.
E_i = initial tangent modulus.
σ_{df} = σ_d at failure.

σ_{df} is determined from the asymptotic values of σ_d that occur near failure (large displacement). By rewriting the hyperbolic equation in a linear form in terms of ε_1/σ_d and ε_1, σ_{df} and E_i can be estimated by inversing the slope and intercept, respectively (figure 2).

$$\frac{\varepsilon_1}{\sigma_d} = \varepsilon_1 \frac{1}{\sigma_{df}} + \frac{1}{E_i}$$

Figure 2. Equation. Hyperbolic relationship in linear form.

During the entirety of the triaxial compression test, which includes the soil behavior near failure, σ_d and corresponding ε_1 are measured. Therefore, fitting a linear line through available measured data (i.e., ε_1/σ_d versus ε_1) enables the determination of the hyperbolic stress–strain relationship for the entire loading process. Similarly, multiple datasets of σ_d and ε_1 induced in a representative element of an SG layer resulting from multiple FWD load levels can be input into the hyperbolic equation. FWD load levels are not expected to reach the failure state, which means fitting a line through available datasets of σ_d and ε_1 in essence extrapolates the measured data up to the failure conditions (i.e., the asymptotic value) (figure 3 and figure 4). In other words, identifying an equivalent triaxial condition for the representative element of an SG layer under FWD loading can lead to the estimation of σ_{df}.

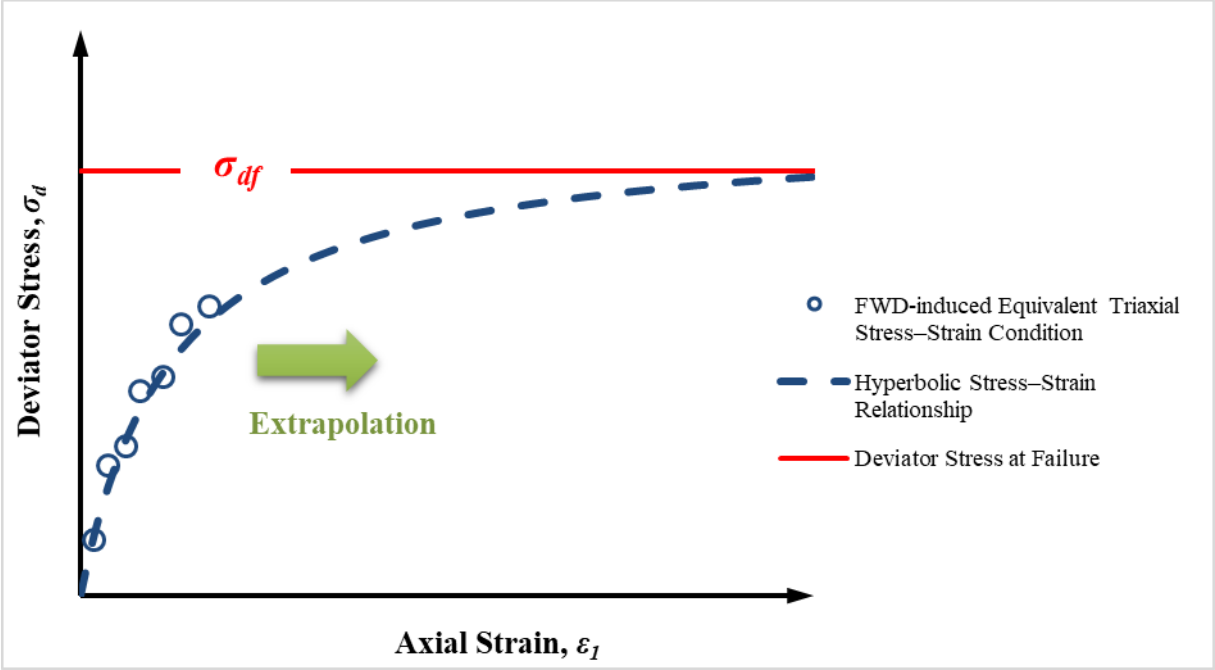

Figure 3. Illustration. Extrapolation of hyperbolic relationship.

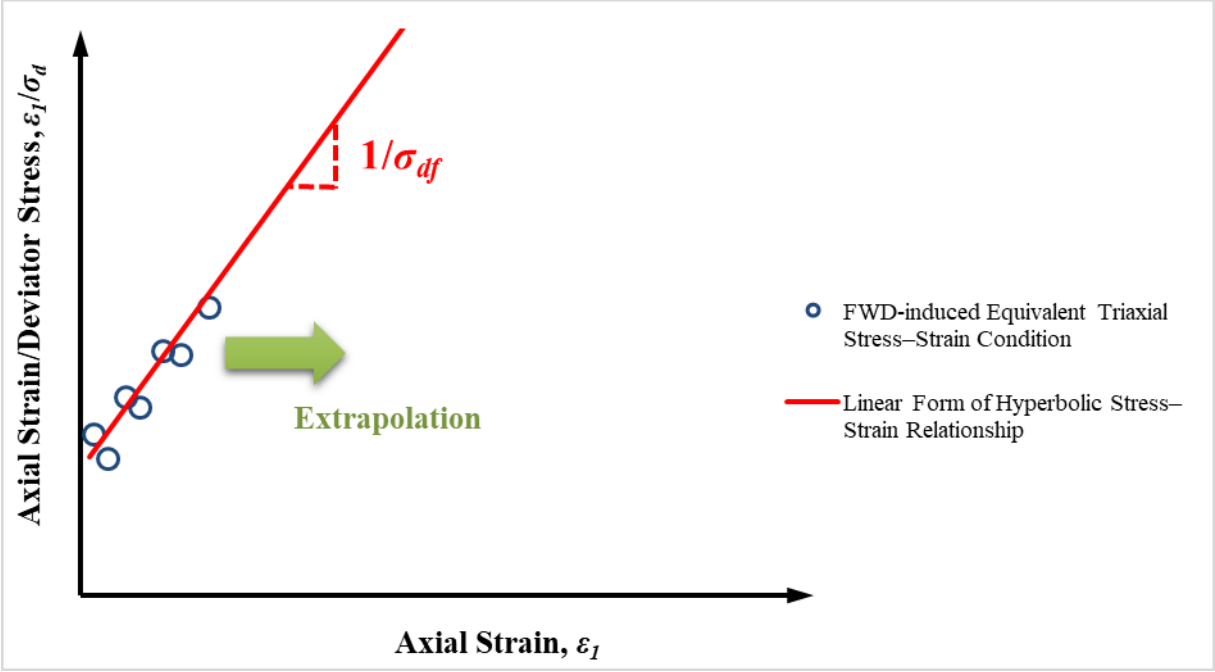

Figure 4. Illustration. Estimation of σ_{df} using linear form of hyperbolic relationship.

2.2. EQUIVALENT TRIAXIAL CONDITION UNDER FWD LOADING

It is commonly accepted that the M_R of unbound materials, such as crushed aggregate base (CAB) and SG soils, is a function of the stress conditions. Such a characteristic of these materials is usually reflected in the backcalculated moduli when multiple load levels are applied.[12] The set of backcalculated SG moduli at different load levels, in conjunction with the corresponding computed load-induced state of stresses, are utilized in the proposed procedure to determine the multiple datasets of σ_d and ε_1. These determined sets of values are then used to fit a hyperbolic relationship (figure 1 and figure 2). The following steps outline the proposed approach:

1. The backcalculated layer moduli at each load level are used with a layered linear elastic program (LEP) to compute the stress tensor (σ_{ij}) at a representative element in an SG layer. An element located at the depth of $B_{FWD}/2$ (B_{FWD} is the FWD-plate diameter) from the top of an SG layer and centerline of the load can be viewed as the representative element to determine the load-induced stresses. The representative element (at $B_{FWD}/2$ from the top of an SG surface) is bounded by shearing zones in the SG and experiences the largest vertical strain under the circular loaded area.[13] Note that incorporating backcalculated layer moduli with an LEP has been a conventional step in mechanistic–empirical pavement-analysis and -design procedures to obtain the needed critical pavement responses.[14]

2. The calculated induced σ_{ij} at the representative element are transformed into equivalent laboratory triaxial-stress testing conditions via stress invariants similar to previous studies.[15–17] Stress invariant values are the same regardless of the orientation of the coordinate system chosen. The octahedral normal stress (σ_{oct}) and octahedral shear stress (τ_{oct}), which are also invariants, are used to convert the σ_{ij} computed in the representative SG element under the FWD loads to σ_d and confining stress (σ_c) in a triaxial-testing setup using the equations presented in figure 5 through figure 8. In these equations, σ_1, σ_2, and σ_3 are the major, intermediate, and minor principal stresses, respectively.

$$\sigma_{oct} = \frac{1}{3}(\sigma_1 + \sigma_2 + \sigma_3)$$

Figure 5. Equation. Calculation of σ_{oct} using principal stresses.

$$|\tau_{oct}| = \frac{1}{3}\sqrt{(\sigma_1 - \sigma_2)^2 + (\sigma_2 - \sigma_3)^2 + (\sigma_3 - \sigma_1)^2}$$

Figure 6. Equation. Calculation of τ_{oct} using principal stresses.

$$\sigma_d = \frac{3}{\sqrt{2}}|\tau_{oct}|$$

Figure 7. Equation. σ_d calculation using τ_{oct}.

$$\sigma_c = \sigma_{oct} - \frac{\sigma_d}{3}$$

Figure 8. Equation. σ_c calculation using σ_{oct}.

3. Calculated σ_d values at each load level are then used to compute the corresponding triaxial ε_1 as expressed by the equation in figure 9, where $(M_R)_{SG}$ is the backcalculated SG M_R at the corresponding load level.

$$\varepsilon_1 = \frac{\sigma_d}{(M_R)_{SG}}$$

Figure 9. Equation. ε_1 calculation.

4. Using the linear fit of computed multiple datasets of σ_d and ε_1, the σ_{df}, which is equal to the inverse slope of ε_1/σ_d versus ε_1, can be determined. In a case when the $(M_R)_{SG}$ decreases with increasing load level (i.e., dominant softening behavior), the slope of ε_1/σ_d versus ε_1 is positive, which is a characteristic of fine-grained soil. On the other hand, a negative slope indicates a hardening behavior. In such a case, there is no asymptotic value that represents failure, and therefore, the proposed approach would not be applicable.

5. Based on the determined σ_{df} and computed average of σ_c ($\sigma_{c\text{-}avg}$) at each load level (figure 8), it is possible to establish only one Mohr circle of failure. Hajj et al. showed that the variation of σ_c values at different load levels given by the equation in figure 8 was low (within 10 percent), indicating that a single $\sigma_{c\text{-}avg}$ value may be appropriate.[15] Accordingly, a range of SG c values can be estimated using the equation in figure 10 by assuming an acceptable range for ϕ based on the known soil classification of the SG. It may be noted that reliable data exist in the literature for selecting an appropriate range of ϕ based on soil classification.[18–21]

$$\sigma_1 = \sigma_{c\text{-}avg} + \sigma_{df} = \sigma_{c\text{-}avg} \cdot tan^2(45 + \phi/2) + 2c \cdot tan(45 + \phi/2)$$

Figure 10. Equation. Determining SG strength parameters (ϕ and c).

Note that using linear-elastic theory, in conjunction with FWD measurements, is common practice to evaluate in-situ M_R of pavement layers. Subsequent determination of load-induced state of stresses and strains using LEP also uses the same set of assumptions (i.e., stationary–static axisymmetric loading). However, the stress dependency of SG material is incorporated in the process as it employs the $(M_R)_{SG}$ obtained from multiple FWD load levels.[12]

CHAPTER 3. VALIDATION OF PROPOSED METHODOLOGY

To validate the proposed FWD-based methodology, the applicability of extrapolating datasets of σ_d and ε_1 to the near-failure level to estimate σ_{df} is investigated first. Afterward, numerical simulation of FWD testing as well as field FWD measurements conducted on a variety of unpaved and paved pavement structures were employed to verify the applicability of the proposed procedure.

3.1. EXTRAPOLATION OF HYPERBOLIC RELATIONSHIP

As stated in section 2.1, FWD load levels and associated states of stress in the SG layer do not reach the failure state of the materials. The extension of the data obtained at lower stress levels to the failure state enables the estimation of maximum σ_d (asymptotic value). However, extrapolation of the hyperbolic relationship using the measured data at lower states of stress should be examined by means of measured triaxial test results.

To this end, the results of consolidated undrained triaxial tests without pore-water measurements conducted on two different types of soils were employed. The first soil (SG I) used as the SG material in large-scale experiments in this study was clayey sand with gravel (SC) with a ϕ of 38 degrees and c of 2 psi. The second soil (SG II) is called Dupont clay with a ϕ of 18 degrees and c of 3.5 psi, which has been used in the National Airport Pavement Test Facility (NAPTF) of the Federal Aviation Administration (FAA).[22] Figure 11 and figure 12 show σ_d versus ε_1 for SC soil and Dupont clay at different confining pressures, respectively. Triaxial test results for the SC soil were available at only two confining pressures.

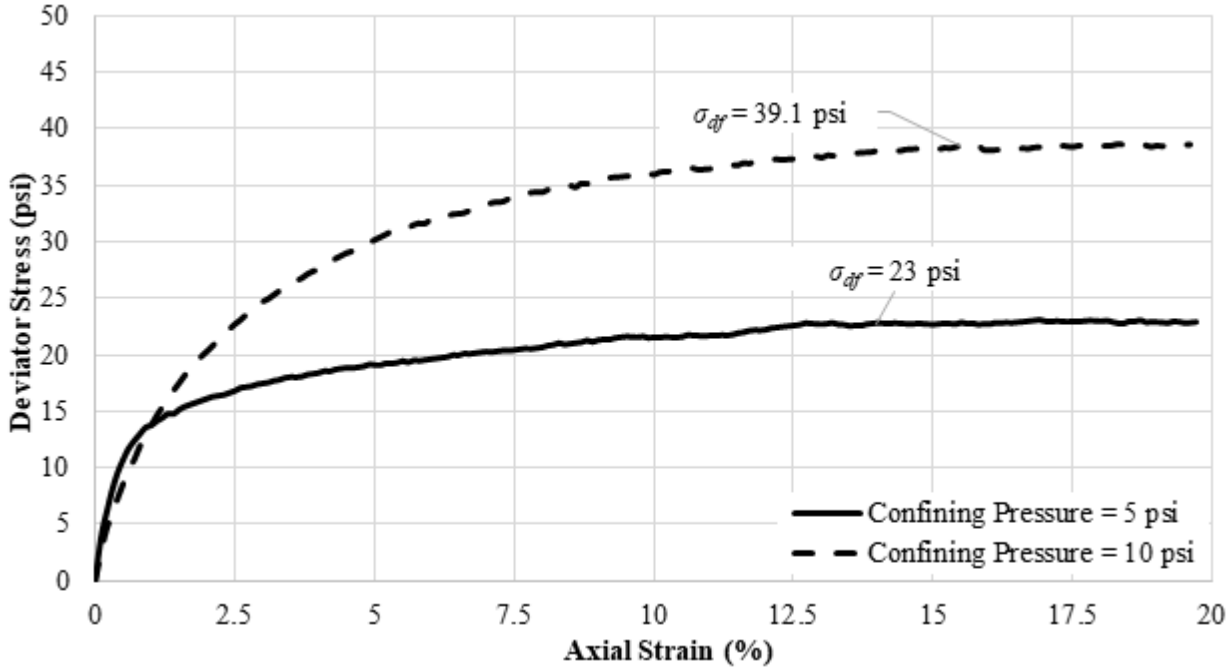

Figure 11. Graph. Result of triaxial tests on SC.

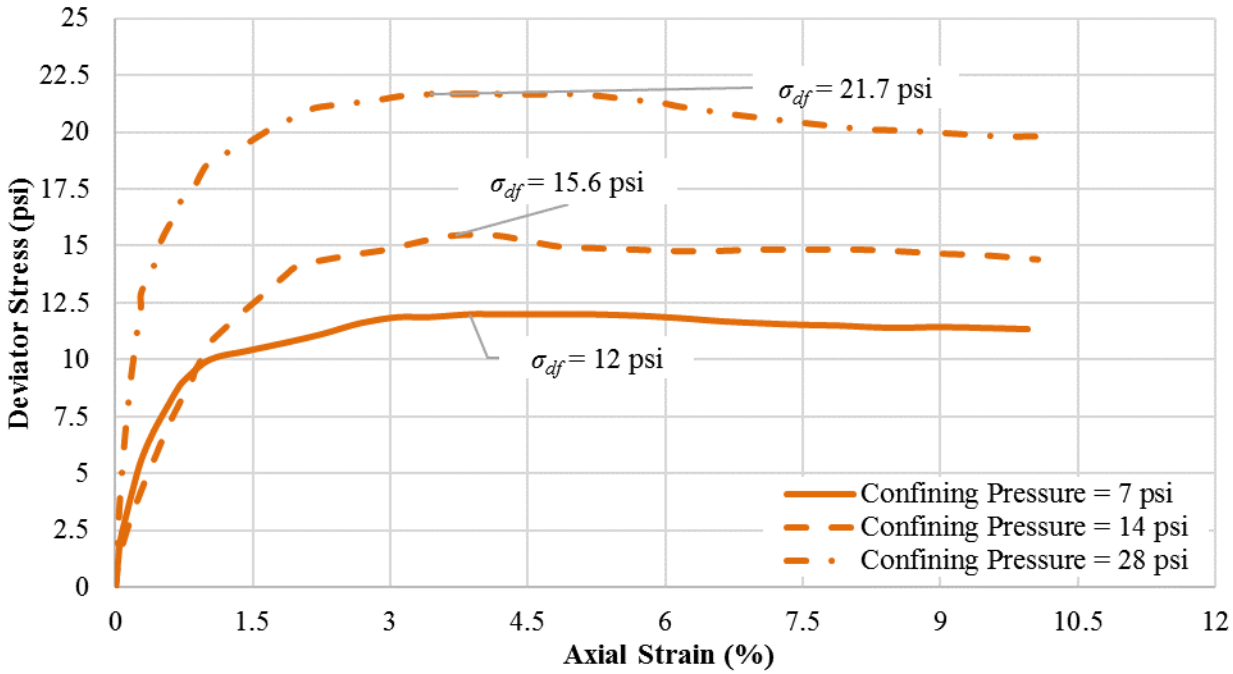

Figure 12. Graph. Result of triaxial tests on Dupont clay.

For each set of triaxial-test results, σ_d up to the cutoff levels of 20, 30, 40, and 50 percent of σ_{df} and corresponding ε_1 were separately used to develop the linear form of hyperbolic relationship (figure 2). Consequently, the estimated σ_{df} (i.e., inverse slope) was determined using many sets of truncated data. Figure 13 and figure 14 depict the estimated σ_{df} normalized by the measured σ_{df} (from triaxial tests) for different cutoff levels of 20, 30, 40, and 50 percent of the measured σ_{df}.

As presented in figure 13 and figure 14, regardless of soil type and confining pressure, the use of measured data from a higher cutoff level results in better estimates for σ_{df}. In other words, by engaging more data points of σ_d and ε_1, better estimation of σ_{df} is possible. It can be seen that, at the cutoff level of 50 percent, the estimated σ_{df} is reasonably close to the measured value (i.e., less than a 15-percent difference). Thus, it can be concluded that, when the state of σ_d in a triaxial test reaches approximately 50 percent of σ_{df}, a hyperbolic relationship can be utilized to obtain the needed asymptotic value.

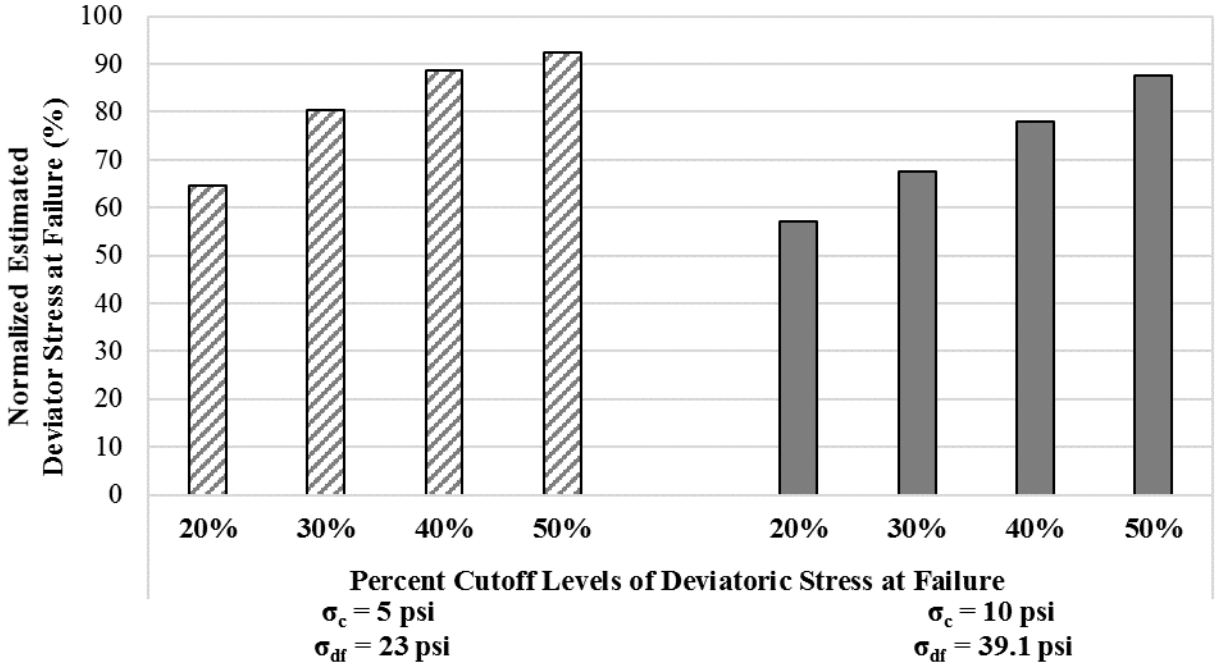

Figure 13. Bar chart. Normalized estimated σ_d using datasets at different cutoff levels of measured data for SC.

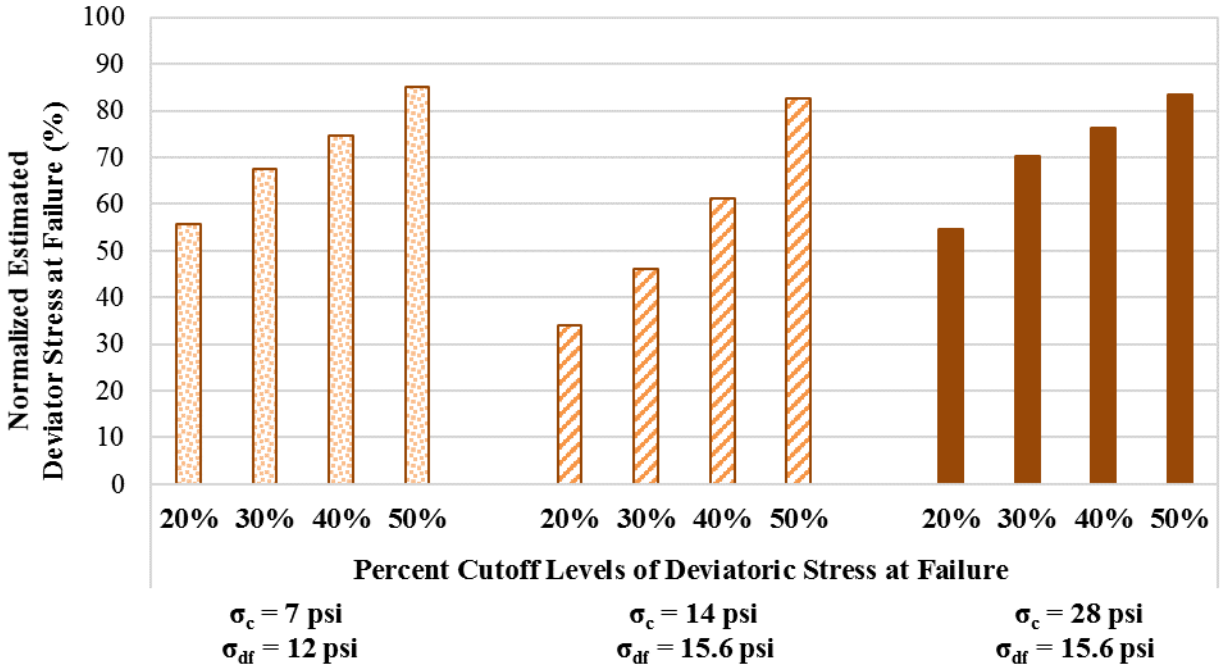

Figure 14. Bar chart. Normalized estimated σ_d using datasets at different cutoff levels of measured data for Dupont clay.

3.2. ESTIMATION OF SG STRENGTH PARAMETERS: SINGLE SG LAYER

In this section, verification of the proposed methodology for estimating SG shear strength parameters by applying FWD-type loading directly on top of an SG is presented. Numerical modeling of FWD testing as well as field FWD measurements collected from the large-scale experiment (experiment No. 1) and light weight deflectometer (LWD) measurements obtained from NAPTF were used. The applied load levels in the numerical simulation and large-scale experiment are the typical range that can be handled by LWD devices. The concept behind the LWD device is very similar to the FWD device, but the impulse load levels are lower, and it is often used with unbound materials.

3.2.1. Numerical Modeling of FWD Testing: Single SG Layer

In order to investigate the validity of the proposed methodology, a numerical simulation of FWD testing using ILLI-PAVE software was conducted. The main advantages of ILLI-PAVE software are substantially lower computational effort because of the use of axisymmetric finite element formulation and the consideration of stress dependency (nonlinearity) along with failure conditions (ϕ and c) of unbound materials.[23] SG responses under LWD-type loading for two SG materials, SG I and SG II, with different properties were simulated. To capture stress-dependent behavior of SG materials, a bilinear (arithmetic) model (figure 15), the Uzan model (figure 16), and representative shear strength parameters were selected for SG I and SG II, respectively. Material properties, which were adopted from the literature and used in the current analysis, are summarized in table 2 for SG I and SG II.[23,24]

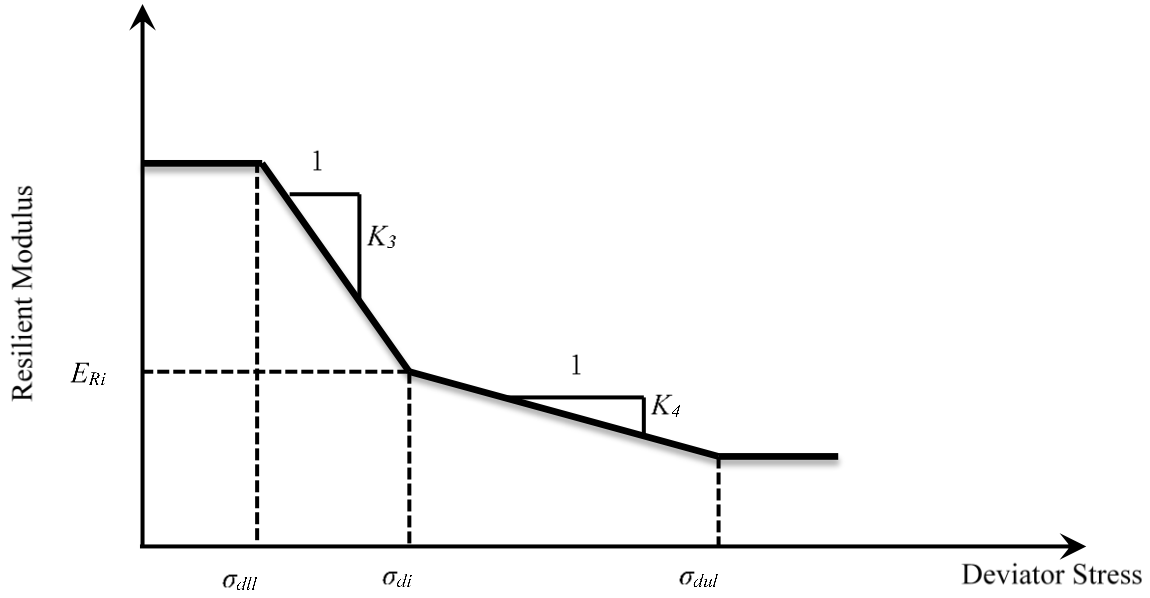

E_{Ri} = breakpoint M_R; $\sigma_{dll} = \sigma_d$ lower limit; σ_{di} = breakpoint σ_d; $\sigma_{dul} = \sigma_d$ upper limit; K_3 = slope of linear in bilinear model before σ_{di}; K_4 = slope of linear in bilinear model after σ_{di}.

Figure 15. Illustration. Bilinear model for representing stress dependency of unbound materials.

$$M_R = K\theta^n \sigma_d^m$$

Figure 16. Equation. Uzan model for representing stress dependency of unbound materials.

Where:

θ = bulk stress.
K = regression constant of M_R model.
n = θ exponent.
m = σ_d exponent.

Table 2. Material properties and layer thicknesses of SG I and SG II.

Property	SG I	SG II
Layer thickness (inches)	276	276
Density (pcf)	100	100
K_0	0.85	0.80
M_R model	Bilinear model	Uzan model
M_R model constants	σ_{di} = 6.2 psi E_{Ri} = 3,000 psi K_3 = 1,110 psi/psi K_4 = −178 psi/psi σ_{dll} = 2 psi σ_{dul} = 12.9 psi	K = 1,793 psi n = 0.19 m = −0.36
ν	0.45	0.45
ϕ (degrees)	0	12
c (psi)	7	19

K_0 = lateral earth pressure coefficient; σ_{di} = breakpoint σ_d; E_{Ri} = breakpoint M_R; K_3 = slope of linear in bilinear model before σ_{di}; K_4 = slope of linear in bilinear model after σ_{di}; σ_{dll} = σ_d lower limit; σ_{dul} = σ_d upper limit; ν = Poisson's ratio.

The LWD tests were simulated by applying various loads (500; 1,000; 1,500; 2,000; 2,500; and 3,000 lb) on a circular plate with a 5.91-inch radius. The corresponding surface displacements at 0, 8, and 12 inches away from the center of the loading plate were computed (figure 17 and figure 18).

As the proposed methodology relies on the stress dependency and softening behavior of SG material (i.e., positive ε_1/σ_d versus ε_1 relationship), such characteristics of an SG layer should be examined first. A methodology based on deflection ratio (DR) was used for investigating the nonlinearity in pavement layers (e.g., SG only). DR can be calculated by dividing the normalized deflections under the higher load level by the normalized deflections under the initial load level (i.e., 500 lb). This methodology is capable of capturing the stress-hardening or -softening characteristic of materials at different radial distances.[25] A DR value of 1.0 indicates linear-elastic behavior for the unbound material. Figure 19 and figure 20 depict the calculated DR values for SG I and SG II, respectively, at different locations (i.e., 0, 8, and 12 inches away from the center). An increase in DR when applying higher load levels can be inferred from this figure, indicating a dominant softening behavior in the SGs under consideration.

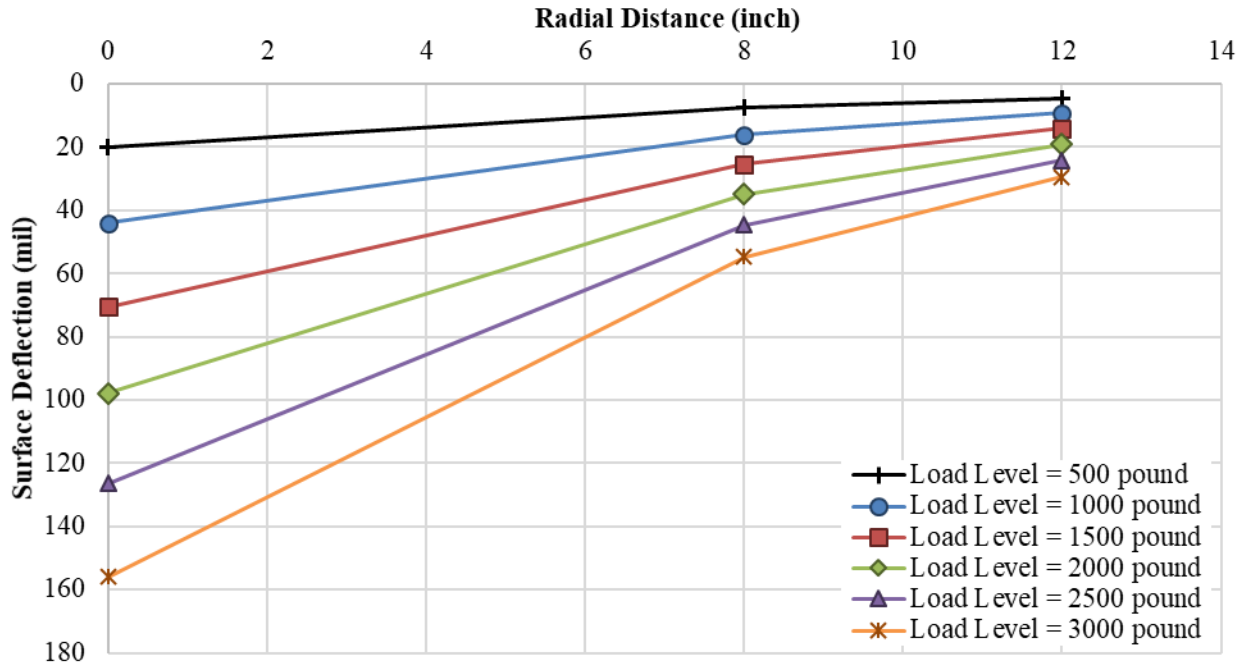

Figure 17. Graph. Computed surface deflections of SG I under LWD loadings.

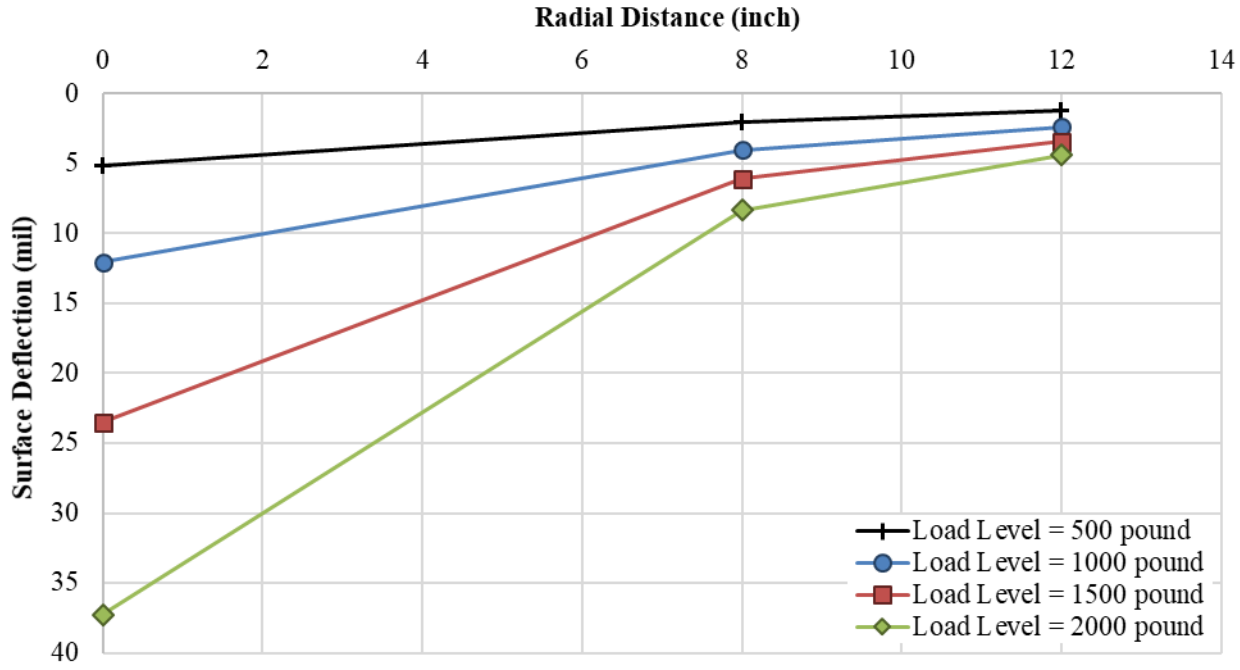

Figure 18. Graph. Computed surface deflections of SG II under LWD loadings.

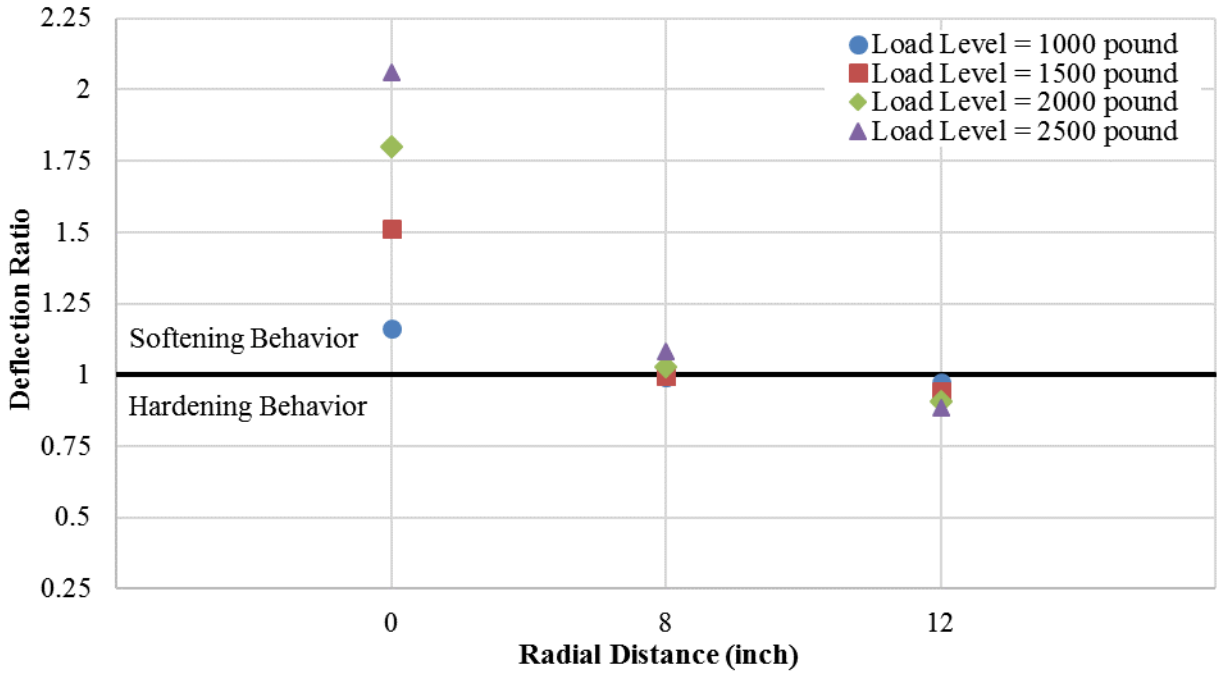

Figure 19. Graph. Evaluation of nonlinearity in SG I.

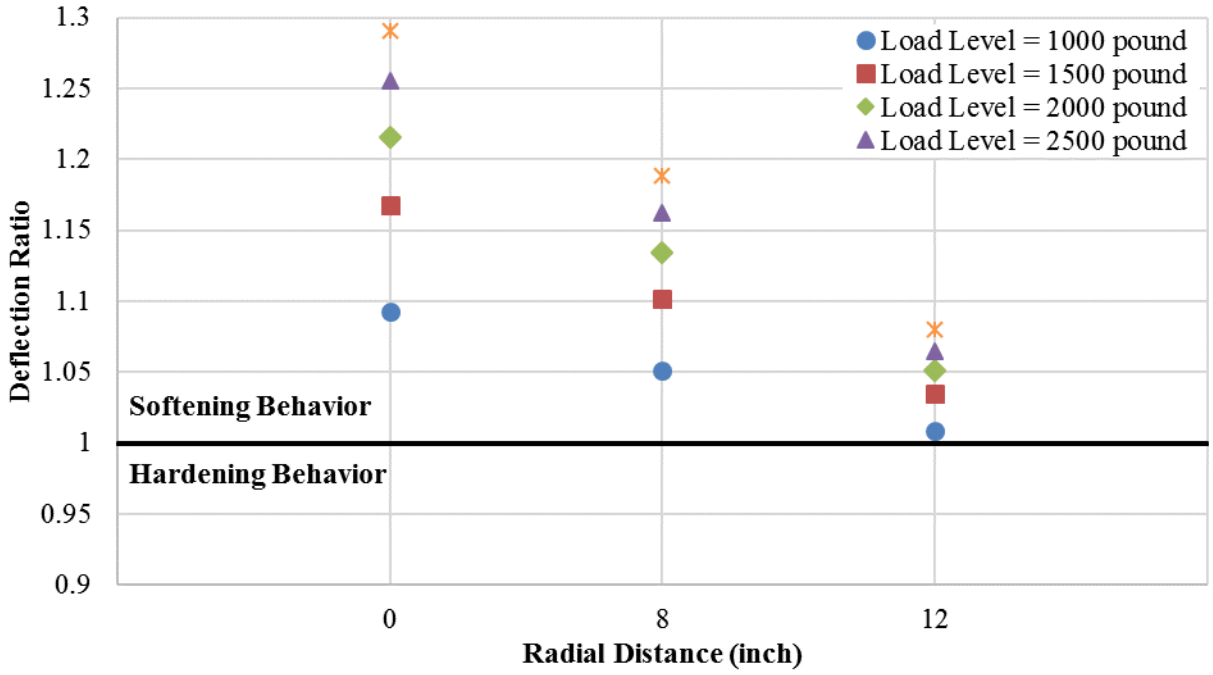

Figure 20. Graph. Evaluation of nonlinearity in SG II.

To undertake the backcalculation process, the opensource BAKFAA software was utilized.[26] Repeated attempts at the backcalculation process with many controls on the variability of the elastic modulus revealed that the SG layer should be divided into two sublayers using the Depth to an Apparent Rigid Layer Method.[27] This procedure enables the consideration of the stress

dependency of unbound material in backcalculation. The outputs of backcalculation for both SGs revealed that the increase in LWD load level resulted in the reduction in $(M_R)_{SG}$, indicating a softening behavior, which is consistent with the DR analysis.

Based on the backcalculated moduli at each of the load levels, the σ_{ij} at 5.9 inches (i.e., $B_{FWD}/2$) below the SG surface was computed by assuming static loading conditions using the 3D-Move Analysis software.[28] σ_{df}, which is equal to the inverse slope of ε_1/σ_d versus ε_1, can be estimated using the transformation of the stress condition to the corresponding triaxial testing condition. As stated in section 2.2, by assuming a range of values for ϕ, the corresponding c values can be determined for SGs. For a ϕ equal to 0 degrees for SG I and a ϕ equal to 12 degrees for SG II, which are the values used in the ILLI-PAVE simulations,
c values of 7.8 and 19.4 psi were determined for SG I and SG II, respectively.[23] These sets of estimated c values are consistent with the assumed c of 7 and 19 psi, which were used in ILLI-PAVE simulations.

The calculated σ_d at the highest load level were 39 and 31 percent of the estimated σ_{df} for SG I and SG II, respectively. Even though these values were less than 50 percent of the estimated σ_{df}, this simulation exercise implies that the proposed approach of incorporating nonlinear behavior of SG with the hyperbolic stress–strain relationship can provide a good estimation of an SG's c when an appropriate range of ϕ is assumed. The calculations associated with the proposed approach for SG I and SG II are summarized in table 3 and table 4. The analysis was stopped at the load level of 2,000 lb for SG I and 3,000 lb for SG II because gradual increases in the applied load and subsequent calculations revealed negligible (less than 5 percent) increases in the estimated σ_d beyond these load levels.

Table 3. Estimation process of shear strength parameters for SG I and SG II.

Material	Load Level (lb)	$(M_R)_{SG}$ (psi)	σ_1 (psi)	σ_2 (psi)	σ_3 (psi)	σ_{oct} (psi)	τ_{oct} (psi)	σ_d (psi)	ε_1 (Micro-strain)	ε_1/σ_d
SG I	500	7,962	2.95	0.47	0.46	1.29	1.17	1.29	311.9	125.6
SG I	1,000	6,118	6.09	1.06	1.05	2.74	2.37	2.74	823.1	163.4
SG I	1,500	4,098	9.50	1.81	1.80	4.37	3.63	4.37	1,878.4	244.0
SG I	2,000	3,233	12.90	2.55	2.53	5.99	4.88	5.99	3,204.9	309.3
SG II	500	1,965	2.85	0.44	0.43	1.24	1.14	2.42	1,230.9	508.9
SG II	1,000	1,807	5.71	0.88	0.87	2.48	2.28	4.84	2,677.0	553.4
SG II	1,500	1,658	8.56	1.29	1.28	3.71	3.43	7.28	4,393.0	603.1
SG II	2,000	1,594	11.42	1.72	1.70	4.95	4.58	9.71	6,092.6	627.3
SG II	2,500	1,513	14.28	2.11	2.09	6.16	5.74	12.18	8,050.9	660.9
SG II	3,000	1,430	17.14	2.53	2.51	7.39	6.89	14.62	10,223.4	699.3

Table 4. Estimated shear strength parameters for SG I and SG II.

Material	$\sigma_{c\text{-}avg}$ (psi)	σ_{df} (psi)	Normalized σ_d at Highest Load Level With Respect to σ_{df} (%)	ϕ (Degrees)	c (psi)
SG I	1.47	15.6	39	0	7.8
SG II	1.48	48.0	31	12	19.4

3.2.2. Measured Surface-Deflection Data: Single SG Layer

In order to experimentally evaluate the applicability of the developed methodology, a large-scale experiment (experiment No. 1) that included FWD-type testing on the 66-inch SG layer was designed and conducted. Detailed discussion regarding the large-scale experiments (e.g., construction procedure, instrumentation, material properties) conducted as part of this study can be found in Volume II: Appendix A.[(2)]

The SG material was classified as SC. The results of the unsaturated triaxial tests indicated a ϕ of 38 degrees and c of 2 psi. Surface deflections using surface linear variable differential transformers (LVDTs) at the center of loading plate (LVDT1), 8 inches (LVDT2) away from the center of the plate, and 12 inches (LVDT3) away from the center of the plate were measured. In addition to the surface measurements, total earth pressure cells (e.g., P1 and P5) embedded in the SG layer captured the load-induced σ_v during the experiment.

In order to further assess the applicability of the developed methodology, the LWD measurements obtained from Construction Cycle 6 at FAA's NAPTF study were also employed.[(22)] The LWD testing on the compacted Dupont clay SG at two nearby locations along the length of the section was analyzed; each location included four load levels (approximately 600; 800; 1,000; and 1,200 lb). In addition, the study reported the results of strength parameters from triaxial tests as ϕ of 18 degrees and c of 3.5 psi for the Dupont clay SG (figure 12).

Table 5 through table 7 present the surface-deflection recordings measured in experiment No. 1 and the FAA study's location 1 and location 2, respectively.[(22)] As a first step, the stress dependency for the SG layers was examined using the measured surface deflections. Deflection softening behavior was identified in both cases (i.e., experiment No. 1 and the FAA study) according to the DR approach outlined in section 3.2.1 (table 5). The backcalculation process was then conducted by adopting the Depth to an Apparent Rigid Layer Method.[(27)] In the FAA study, the SG modulus was backcalculated using a Boussinesq solution (figure 21) because only the center deflection was available.

Table 5. Surface-deflection measurements in experiment No. 1 and corresponding backcalculated moduli.

Applied Load (lb)	LVDT1 (mil)	LVDT2 (mil)	LVDT3 (mil)	DR at LVDT1	DR at LVDT2	DR at LVDT3	$(M_R)_{SG}$ (psi)	σ_d (psi)	σ_d/σ_{df} (%)
1,154	5.92	5.10	4.79	1.00	1.00	1.00	39,800	5.33	25
1,589	8.50	7.59	6.92	1.04	1.08	1.05	37,200	7.36	35
2,079	12.18	10.76	9.22	1.14	1.17	1.07	31,200	9.70	46
2,514	16.39	13.71	13.08	1.27	1.23	1.25	24,100	11.82	56
3,072	22.62	17.71	16.63	1.43	1.30	1.30	17,500	14.70	70

Table 6. Surface-deflection measurements in the FAA study (location 1) and corresponding backcalculated moduli.[22]

Applied Load (lb)	Center Surface Deflection (mil)	DR	$(M_R)_{SG}$ (psi)	σ_d (psi)	σ_d/σ_{df} (%)
597	5.2	1.00	10,200	3.04	27
796	7.6	1.10	9,300	4.02	36
921	9.3	1.16	8,800	4.68	42
1,258	17.6	1.61	6,400	6.21	55

Table 7. Surface-deflection measurements in the FAA study (location 2) and corresponding backcalculated moduli.[22]

Applied Load (lb)	Center Surface Deflection (mil)	DR	$(M_R)_{SG}$ (psi)	σ_d (psi)	σ_d/σ_{df} (%)
613	2.9	1.00	18,800	3.04	30
811	4.5	1.17	16,100	4.02	40
943	6.7	1.50	12,500	4.68	46
1,251	10.5	1.77	10,600	6.21	61

$$M_R = \frac{2P_{max}\, r(1-v^2)}{\delta_c}$$

Figure 21. Equation. Boussinesq solution used for the backcalculation of SG layer in the FAA study.[22]

Where:

P_{max} = maximum contact pressure.
r = plate radius.
v = Poisson's ratio (assumed to be equal to 0.4).
δ_c = maximum surface deflection at the center.

The correctness of backcalculated moduli at different load levels was confirmed by a review of the calculated root-mean-square error (RMSE), which is a routine practice. Additionally, in the case of experiment No. 1, σ_v at the location of P1 and P5 under different load levels was calculated using the 3D-Move Analysis software along with the corresponding backcalculated layer moduli associated with the load levels under consideration.[28] Figure 22, which presents the calculated versus measured load-induced σ_v in experiment No. 1, indicates a good agreement between the two. These results indicate the reliability of the assumptions (e.g., incorporating apparent rigid layer and stress dependency in the unbound materials) used in the backcalculation exercise.

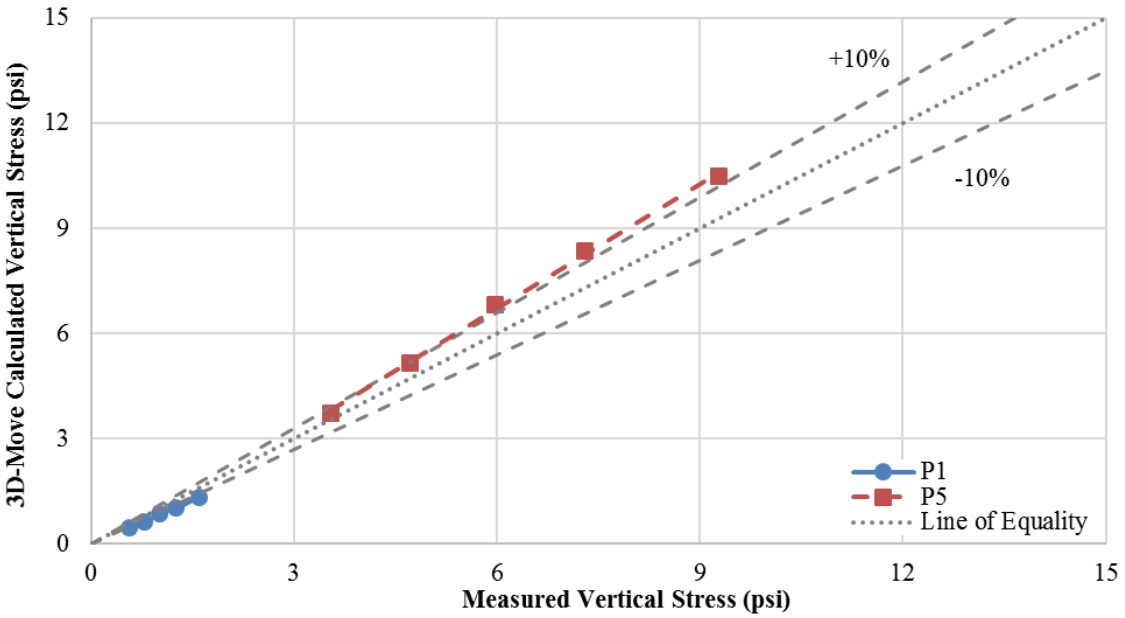

Figure 22. Graph. Comparison between 3D-Move-calculated versus measured σ_v in experiment No. 1.[28]

Using typical ranges for ϕ of the SG-material types used in the experiments (i.e., experiment No. 1 and the FAA study), shear strength parameters can be estimated (table 8).[22] These sets of estimated values, when compared with those obtained from triaxial laboratory testing for the same SG materials, imply that the proposed methodology is capable of estimating the shear strength parameters from in-situ LWD measurements. Reasonable estimations of c for totally different SG material properties support the validity and applicability of the proposed LWD-based methodology. As presented in table 5 through table 7, at the highest load levels in both experiments, the load-induced σ_d at the representative element was higher than 50 percent of the estimated σ_{df}. Caution should be exercised when this value is much lower (below 30 percent) because the extrapolation of the hyperbolic relationship to near-failure condition may not provide proper estimates of σ_{df}. Under such circumstances, the LWD load level needed to induce an acceptable σ_d level in the SG layer can be estimated by extrapolating the data obtained at the lower load levels to reach the target percent of σ_{df}. Consequently, the LWD field testing and associated analysis should be repeated to include such load levels.

Table 8. Surface-deflection measurements in experiment No. 1 and FAA study and corresponding backcalculated moduli.[22]

Experiment	Soil Classification	Typical Values of ϕ (Degrees)[19,20]	Estimated ϕ (Degrees)	Estimated c (psi)	Average of Estimated ϕ (Degrees)	Average of Estimated c (psi)	Measured ϕ (Degrees)	Measured c (psi)
Experiment No. 1	SC	32–42	32 34 36 38 40 42	3.9 3.6 3.2 2.8 2.5 2.1	37.0	3.0	38.0	2.0
FAA study location 1	Dupont clay	12–20	12 14 16 18 20	3.8 3.6 3.4 3.3 3.0	16.0	3.4	18.0	3.5
FAA study location 2	Dupont clay	12–20	12 14 16 18 20	4.3 4.0 3.8 3.6 3.4	16.0	3.8	18.0	3.5

3.3. ESTIMATION OF SG STRENGTH PARAMETERS: TWO LAYERS OF BASE AND SG

In this section, the verification of the proposed methodology using the FWD-type testing in experiment No. 2 is described. The pavement structure in this experiment was composed of CAB and SG. Note that the applied load levels in this experiment are within the typical range that can be handled by an LWD device.

3.3.1. Measured Surface-Deflection Data: Two Layers of CAB and SG

In experiment No. 2, the pavement structure consisted of 6 inches of CAB and 66 inches of SG. Detailed discussion regarding the large-scale experiments (e.g., construction procedure, instrumentation, material properties) conducted as a part of this study can be found in Volume II: Appendix A.[2] Note that, similar to experiment No. 1, SC with ϕ of 38 degrees and c of 2 psi was used as the SG material.

Table 9 presents the surface-deflection recordings measured in experiment No. 2 along with the $(M_R)_{SG}$ at each of the applied load levels. Steps similar to those followed in experiment No. 1 were undertaken. Deflection softening behavior was identified according to the DR approach outlined in section 3.2.1 (table 9). The backcalculation process was then followed by adopting the Depth to an Apparent Rigid Layer Method.[27]

Table 9. Surface-deflection measurements in experiment No. 2 and corresponding backcalculated moduli.

Applied Load (lb)	LVDT1 (mil)	LVDT2 (mil)	LVDT3 (mil)	DR at LVDT1	DR at LVDT2	DR at LVDT3	$(M_R)_{SG}$ (psi)	σ_d (psi)	σ_d/σ_{df} (%)
2,908	7.00	4.36	3.31	1.00	1.00	1.00	36,300	6.83	39
3,960	11.28	4.97	3.57	1.18	0.84	0.79	31,800	9.15	52
5,018	15.72	6.88	4.49	1.30	0.92	0.79	25,400	11.21	64
6,014	19.56	8.24	5.55	1.35	0.91	0.81	19,000	12.80	73
7,061	22.87	10.75	6.24	1.35	1.02	0.78	14,500	14.01	80

σ_v under different load levels at the locations of P1, P6, P9, and P10 was calculated using the 3D-Move Analysis software with the corresponding backcalculated layer moduli associated with the load levels under consideration.[28] Figure 23, which presents the calculated versus measured load-induced σ_v in experiment No. 2, indicates a good agreement between the two. These results indicate the reliability of the assumptions used in the backcalculation exercise, (e.g., incorporating apparent rigid layer and stress dependency in the unbound materials).

The estimated shear strength parameters for the SG materials are presented in table 10. These sets of estimated values are reasonably close to those obtained from triaxial laboratory testing, which indicates the ability of the proposed methodology for estimating shear strength parameters of SG when the FWD loading is applied on top of CAB.

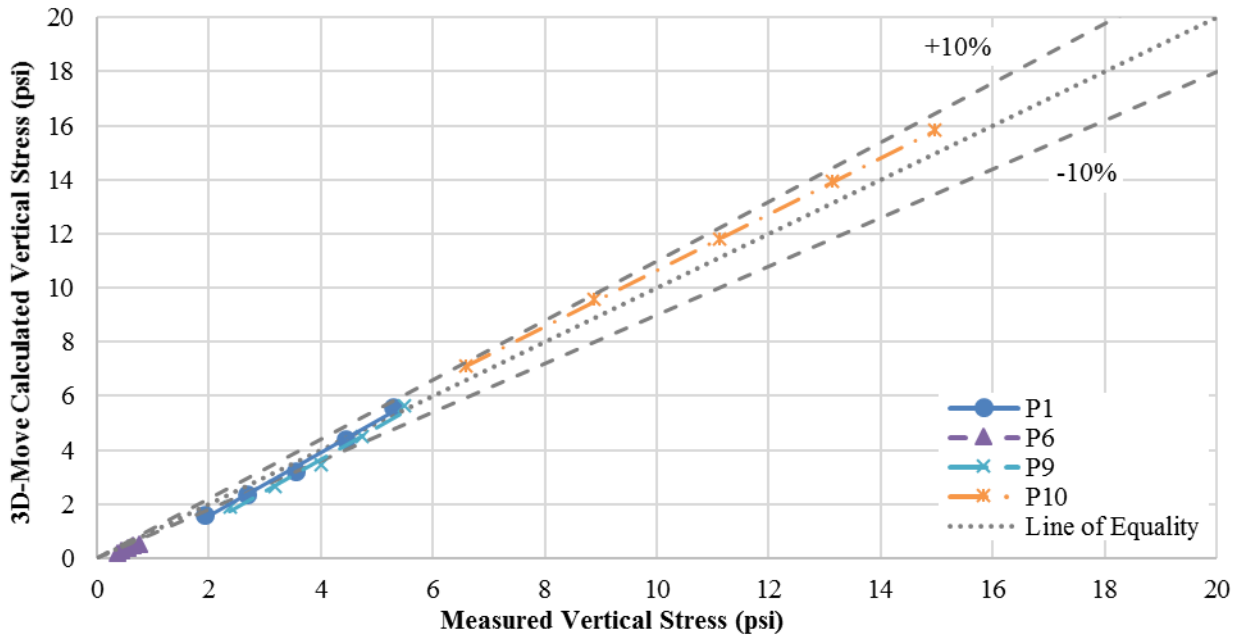

Figure 23. Graph. Comparison between 3D-Move-calculated versus measured σ_v in experiment No. 2.

Table 10. Shear strength parameters estimation for SG materials used in experiment No. 2.

Experiment	Soil Classification	Typical Values of ϕ (Degrees)[20]	Estimated ϕ (Degrees)	Estimated c (psi)	Average of Estimated ϕ (Degrees)	Average of Estimated c (psi)	Measured ϕ (Degrees)	Measured c (psi)
Experiment No. 2	SC	32–42	32	3.7	37.0	2.9	38.0	2.0
			34	3.4				
			36	3.1				
			38	2.8				
			40	2.5				
			42	2.2				

3.4. ESTIMATION OF SG STRENGTH PARAMETERS: AC PAVEMENT

In this section, the verification of proposed methodology using FWD-type testing conducted on pavement structures, including the asphalt concrete (AC) layer (i.e., conventional flexible pavement), is presented. Numerical modeling of FWD testing as well as field FWD measurements collected from the large-scale experiment (experiment No. 3) and APT facility at University of Costa Rica (LanammeUCR) were used as a part of the verification process.

3.4.1. Numerical Modeling of FWD Testing: AC Pavement

The validity of the proposed FWD-based methodology was investigated using the numerical simulation of FWD tests. Synthetic pavement responses under FWD loading were generated using the ILLI-PAVE program.[23]

The FWD simulation was conducted on two different hypothetical pavement structures (PS I and PS II) with different layer thicknesses. Layer thicknesses and material properties used in the simulation are summarized in table 11. As shown, the AC layer was represented with constant linear-elastic properties. In order to capture stress-dependent behavior of unbound materials, the Theta model (figure 24) for CABs, bilinear model (figure 15), and Uzan model (figure 16) along with representative shear strength parameters were selected for the SG layers in PS I and PS II, respectively. Material properties of unbound materials were adopted from the literature.[23,29]

Table 11. Material properties and layer thicknesses of the hypothetical pavement structures.

Properties	AC (PS I)	CAB (PS I)	SG (PS I)	AC (PS II)	CAB (PS II)	SG (PS II)
Layer thickness (inches)	9	10	276	6	8	276
Density (pcf)	145	135	100	145	120	100
K_0	0.67	0.36	0.85	0.67	0.36	0.80
M_R model	Linear elastic	Theta model	Bilinear model	Linear elastic	Theta model	Uzan model
M_R model constants	500,000 psi	K = 9,000 n = 0.33	σ_{di} = 6.2 psi E_{Ri} = 3,000 psi K_3 = 1,110 psi/psi K_4 = –178 psi/psi σ_{dll} = 2 psi σ_{dul} = 12.9 psi	300,000 psi	K = 5,358 n = 0.32	K = 1,793 psi n = 0.19 m = –0.36
v	0.35	0.35	0.45	0.35	0.35	0.45
ϕ (degrees)	—	45	0	—	39	12
c (psi)	—	0	7	—	0	19

—Not applicable.

K_0 = lateral earth pressure coefficient; σ_{di} = breakpoint σ_d; E_{Ri} = breakpoint M_R; K_3 = slope of linear in bilinear model before σ_{di}; K_4 = slope of linear in bilinear model after σ_{di}; σ_{dll} = σ_d lower limit; σ_{dul} = σ_d upper limit.

$$M_R = K\theta^n$$

Figure 24. Equation. Theta model for representing stress dependency of unbound granular materials.

The FWD tests were simulated by applying various loads (9,000; 12,000; 16,000; 21,000; and 27,000 lb) on a circular plate with a 5.91-inch *r*. The corresponding pavement-surface displacements at 0, 8, 12, 18, 24, 36, 48, 60, and 72 inches away from the center of the FWD plate were computed. Figure 25 and figure 26 show the deflection basins of the hypothetical PS I and PS II under the applied load levels, respectively.

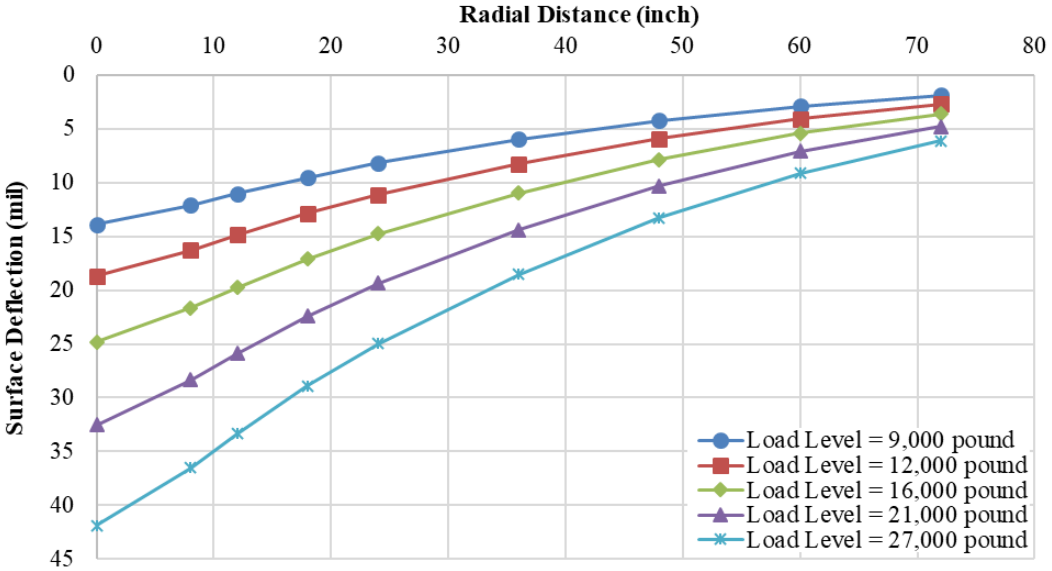

Figure 25. Graph. Deflection basin at different load levels for PS I.

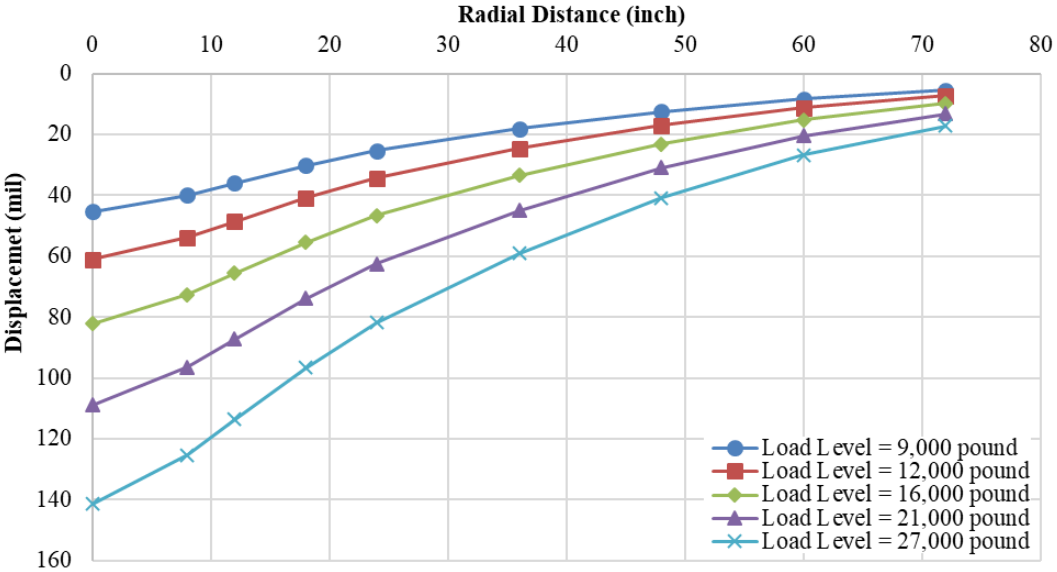

Figure 26. Graph. Deflection basin at different load levels for PS II.

Figure 27 and figure 28 depict the calculated DRs at different locations (i.e., 0, 24, and 60 inches away from the center) for PS I and PS II, respectively. The softening behavior (DR greater than 1) is not only observed at the center; it also increases with increasing radial distances. This observation reveals the dominant softening behavior in the SG because linear-elastic properties for AC layer and hardening constitutive model (Theta) for CAB material were assumed in ILLI-PAVE simulations.[23]

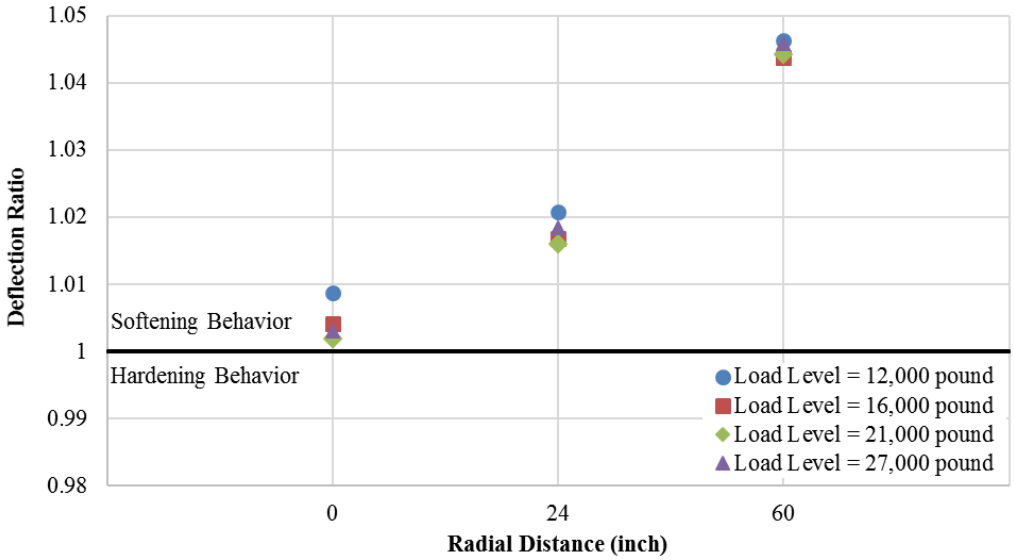

Figure 27. Graph. Evaluation of nonlinearity in the hypothetical PS I using DR at different radial distances.

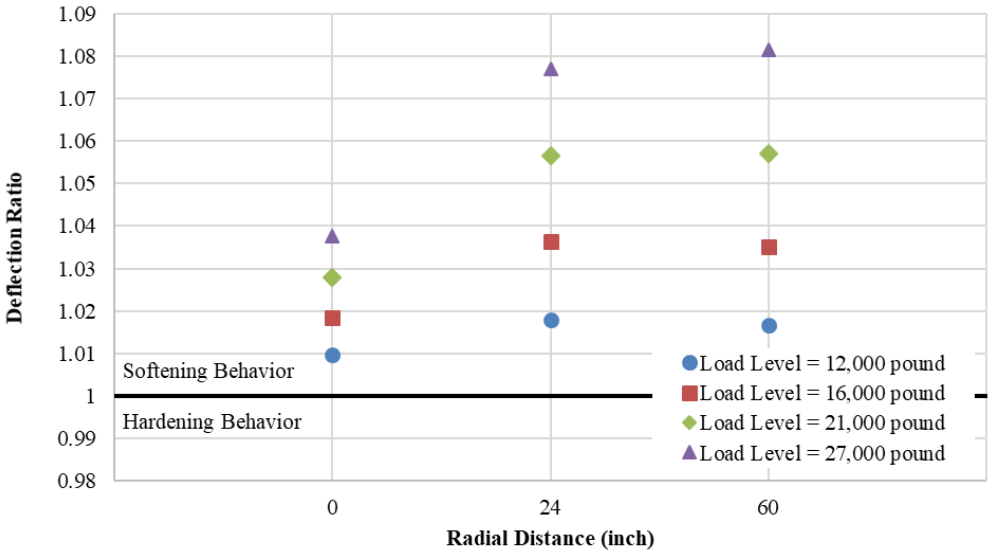

Figure 28. Graph. Evaluation of nonlinearity in the hypothetical PS II using DR at different radial distances.

BAKFAA software was also utilized for the backcalculation of the layers' moduli.[26] It should be mentioned that the assumed constant modulus for the AC layer in the FWD simulation was also specified as input during the backcalculation process. The review of the calculated RMSE during the backcalculation process, which compares the input FWD surface deflections with those that were computed, confirmed the accuracy of the backcalculation exercise.

Figure 29 and figure 30 depict the backcalculated moduli for unbound layers (i.e., CAB and SG) of PS I and PS II, respectively. These figures imply that the increase in FWD load level resulted in the reduction in $(M_R)_{SG}$, indicating the softening material behavior. On the other hand, the increase in the FWD load level resulted in the increase in the base M_R, revealing the hardening behavior of the base material. Such observations are consistent with the DR analysis.

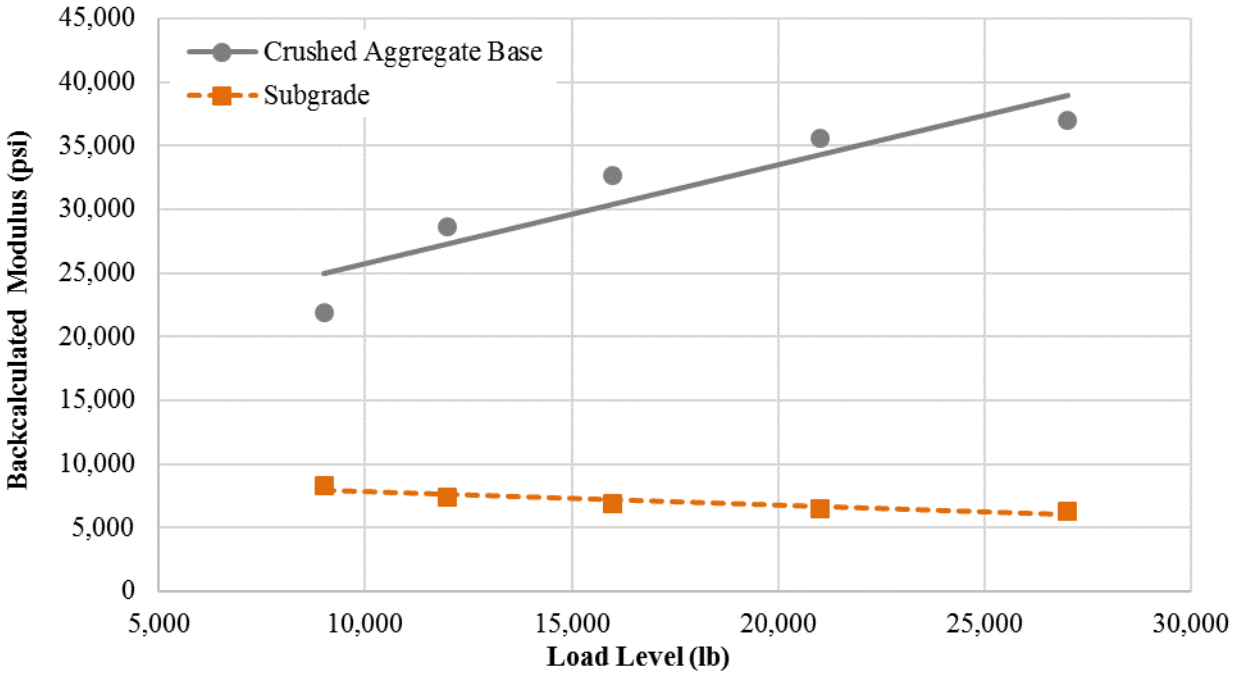

Figure 29. Graph. Backcalculated moduli for the unbound layers of PS I.

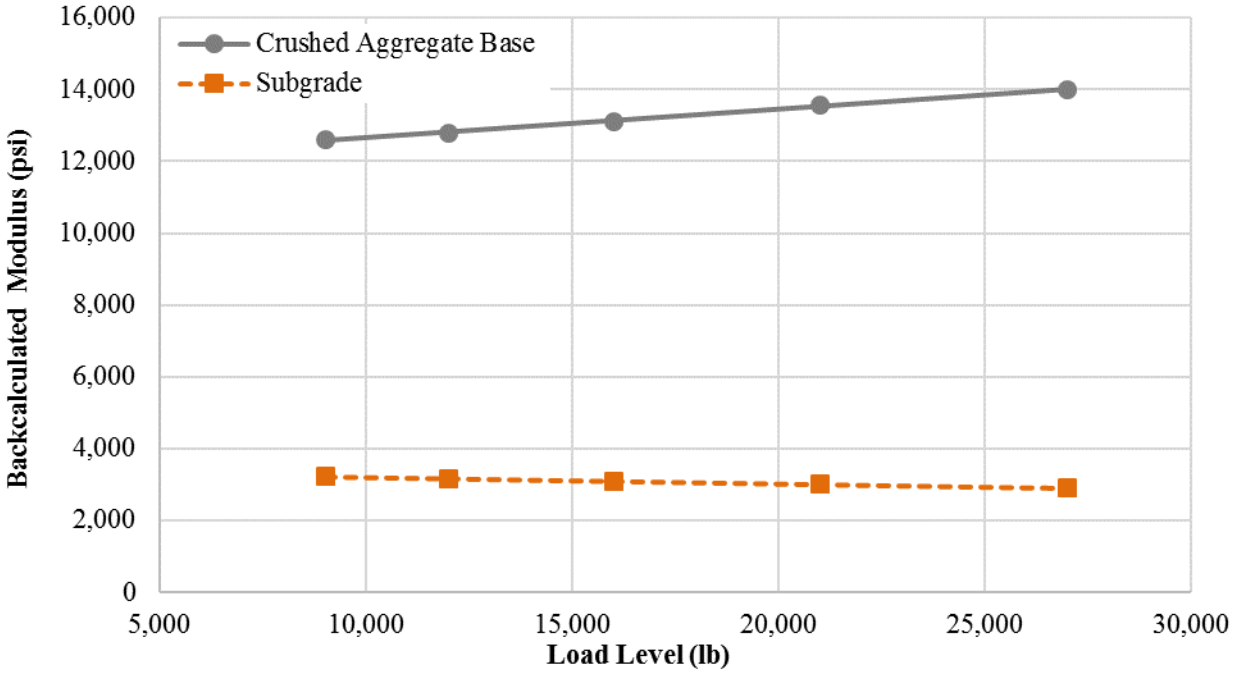

Figure 30. Graph. Backcalculated moduli for the unbound layers of PS II.

σ_{ij} at 5.91 inches (i.e., $B_{FWD}/2$) below the SG surface was computed by assuming static loading conditions using the 3D-Move Analysis software, utilizing the backcalculated moduli at each of the load levels.[28] σ_{df} was then calculated by transforming the stress condition to the corresponding triaxial testing condition (i.e., σ_c and σ_d).

If ϕ were equal to 0 degrees for SG layer in PS I and ϕ were equal to 12 degrees for SG layer in PS II, which were the values used in the ILLI-PAVE simulations, c values of 6.8 and 20.6 psi were determined, respectively.[23] These sets of estimated c values are consistent with the assumed c of 7 and 19 psi in ILLI-PAVE simulations. The results of analysis for PS I and PS II are summarized in table 12 and table 13.

As presented in table 13, the calculated σ_d at the highest load level are 33 and 31 percent of estimated σ_{df} for PS I and PS II, respectively. Although a reasonable estimation of shear strength parameters was obtained by the procedure, caution should be exercised when the load-induced σ_d at the highest load level is less than 30 percent of the estimated σ_{df}. In such cases (e.g., PS II), application of higher FWD load levels may be needed.

Table 12. Shear strength parameters estimation process for PS I and PS II.

Pavement Structure	Load Level (lb)	SG Modulus (psi)	σ_1 (psi)	σ_2 (psi)	σ_3 (psi)	σ_{oct} (psi)	τ_{oct} (psi)	σ_d (psi)	ε_1 (Micro-strain)	ε_1/σ_d
I	9,000	8,405	2.09	0.23	0.23	0.85	0.88	1.86	221.08	118.98
I	12,000	7,362	2.55	0.28	0.28	1.04	1.07	2.27	308.68	135.83
I	16,000	6,873	3.24	0.37	0.37	1.32	1.35	2.87	417.99	145.50
I	21,000	6,553	4.11	0.48	0.48	1.69	1.71	3.63	553.42	152.60
I	27,000	6,336	5.16	0.62	0.62	2.13	2.14	4.54	716.85	157.83
II	9,000	3,245	3.02	0.30	0.30	0.30	1.28	2.72	838.96	308.17
II	12,000	3,170	3.98	0.40	0.40	0.40	1.69	3.58	1,129.91	315.46
II	16,000	3,090	5.22	0.53	0.52	0.53	2.21	4.70	1,520.36	323.62
II	21,000	3,006	6.73	0.68	0.68	0.68	2.85	6.05	2,012.93	332.67
II	27,000	2,923	8.50	0.87	0.86	0.87	3.60	7.63	2,611.04	342.11

Table 13. Estimated shear strength parameters for PS I and PS II.

Pavement Structure	$\sigma_{c\text{-}avg}$ (psi)	σ_{df} (psi)	Normalized σ_d at Highest Load Level With Respect to σ_{df} (%)	ϕ (Degrees)	c (psi)
I	0.4	13.7	33	0	6.8
II	1.48	48.0	31	12	19.4

3.4.2. Measured Surface-Deflection Data: AC Pavement

The applicability of the proposed methodology was experimentally investigated by conducting a large-scale experiment (experiment No. 3) that included FWD testing on the full pavement structure composed of 5 inches of AC, 6 inches of CAB, and 66 inches of SG. Detailed discussion regarding the large-scale experiments (e.g., construction procedure, instrumentation, material properties) conducted as a part of this study can be found in Volume II: Appendix A.[2] Figure 31 shows the surface-deflection measurements in this experiment.

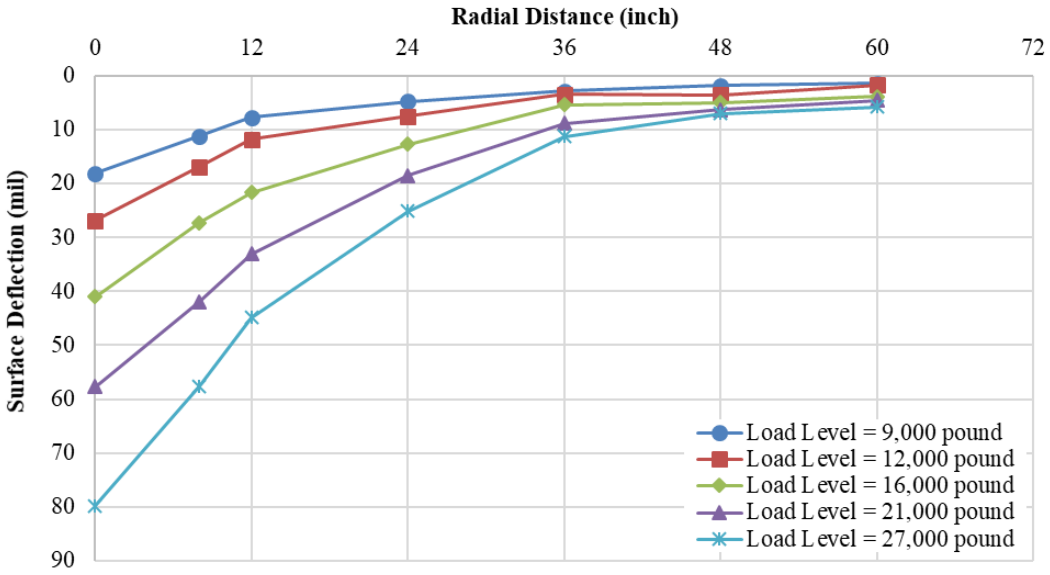

Figure 31. Graph. Deflection basin at different load levels in experiment No. 3.

In order to further assess the applicability of the proposed methodology, the FWD data obtained from LanammeUCR were also utilized. The FWD tests at three load levels (approximately 9,000; 12,000; 16,000 lb) were applied on two pavement structures. These sections, called LanammeUCR-AC2 and LanammeUCR-AC3, were composed of 2.55 and 5.1 inches of an AC layer, respectively. The AC layers in these sections were supported by 9.4 inches of granular base and 11.8 inches of granular subbase materials on top of an SG layer classified as high-plasticity silt with a California bearing ratio of 3. Additionally, the result of triaxial tests reported ϕ of 7 degrees and c of 3.9 psi for the SG material. The FWD measurements at different load levels for LanammeUCR-AC2 and LanammeUCR-AC3 are depicted in figure 32 and figure 33, respectively.

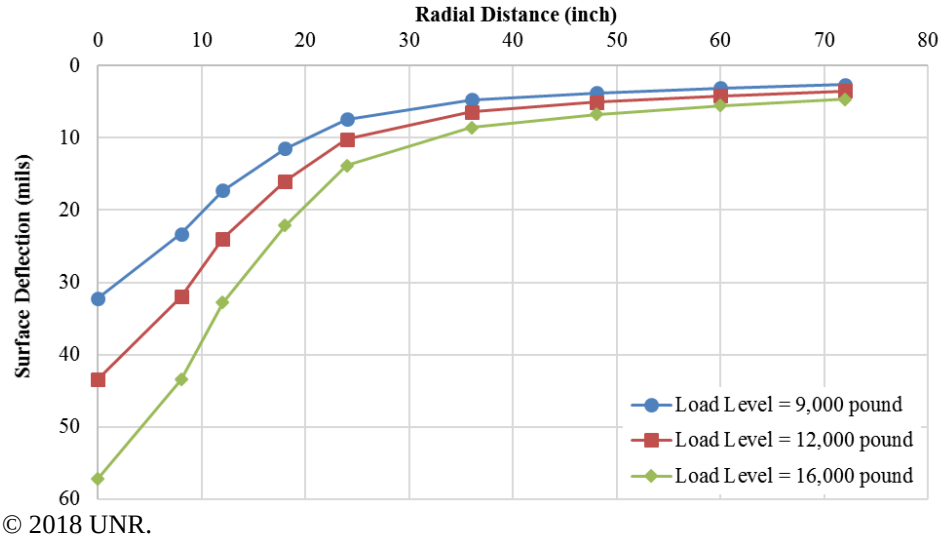

Figure 32. Graph. Deflection basin at load levels in LanammeUCR-AC2.

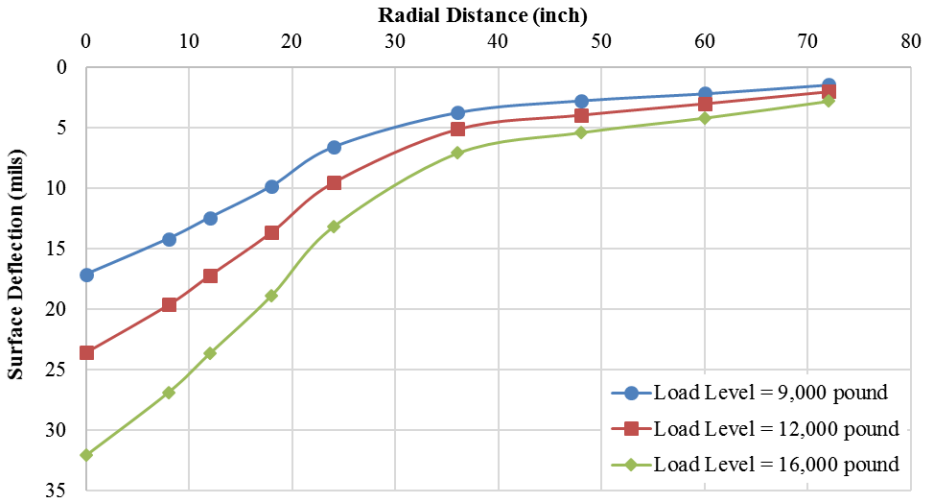

Figure 33. Graph. Deflection basin at load levels in LanammeUCR-AC3.

The stress dependency in the pavement structures was examined using the DR approach (table 14 through table 16). The Depth to an Apparent Rigid Layer Method was adopted for considering the nonlinearity of the SG layer during the backcalculation process.[27] Observation of substantial reduction in the $(M_R)_{SG}$ with increasing the load level confirmed the deflection softening of SG materials.

Table 14. Surface-deflection measurements in experiment No. 3 and corresponding backcalculated moduli.

Applied Load (lb)	LVDT1 (mil)	LVDT5 (mil)	LVDT7 (mil)	DR at LVDT1	DR at LVDT5	DR at LVDT7	$(M_R)_{SG}$ (psi)	σ_d (psi)	σ_d/σ_{df} (%)
8,971	18.11	2.80	1.40	1.00	1.00	1.00	18,500	6.58	30
11,857	26.83	3.42	1.71	1.12	0.93	0.93	16,900	8.35	38
15,860	40.99	5.36	3.82	1.28	1.08	1.55	13,100	10.95	50
21,146	57.72	8.80	4.58	1.35	1.33	1.39	10,000	13.55	62
27,087	79.76	11.24	5.77	1.46	1.33	1.37	7,500	16.46	76

Table 15. Surface-deflection measurements in LanammeUCR-AC2 and corresponding backcalculated moduli.

Applied Load (lb)	LVDT1 (mil)	LVDT5 (mil)	LVDT7 (mil)	DR at LVDT1	DR at LVDT5	DR at LVDT7	$(M_R)_{SG}$ (psi)	σ_d (psi)	σ_d/σ_{df} (%)
8,905	32.22	4.74	3.10	1.00	1.00	1.00	12,200	3.40	32
11,958	43.35	6.39	4.19	1.01	1.01	1.01	10,200	4.27	40
15,247	57.12	8.56	5.50	1.04	1.06	1.03	9,000	5.21	49

Table 16. Surface-deflection measurements in LanammeUCR-AC3 and corresponding backcalculated moduli.

Applied Load (lb)	LVDT1 (mil)	LVDT5 (mil)	LVDT7 (mil)	DR at LVDT1	DR at LVDT5	DR at LVDT7	$(M_R)_{SG}$ (psi)	σ_d (psi)	σ_d/σ_{df} (%)
9,001	15.13	4.21	2.60	1.00	1.00	1.00	11,700	2.26	25
11,686	20.08	5.64	3.44	1.02	1.03	1.01	10,200	2.83	32
15,404	27.70	7.82	4.70	1.07	1.09	1.04	9,300	3.60	40

In order to examine the correctness of the backcalculation process, the load-induced σ_v at the location of pressure cells in experiment No. 3 was calculated using the 3D-Move Analysis software and the corresponding backcalculated layer moduli for the load levels under consideration.[28] Figure 34, which presents the calculated versus measured σ_v for experiment No. 3, indicates a good agreement between the two. These results again imply that the appropriate assumptions (e.g., incorporating apparent rigid layer and stress dependency in the unbound materials) were made in the backcalculation process.

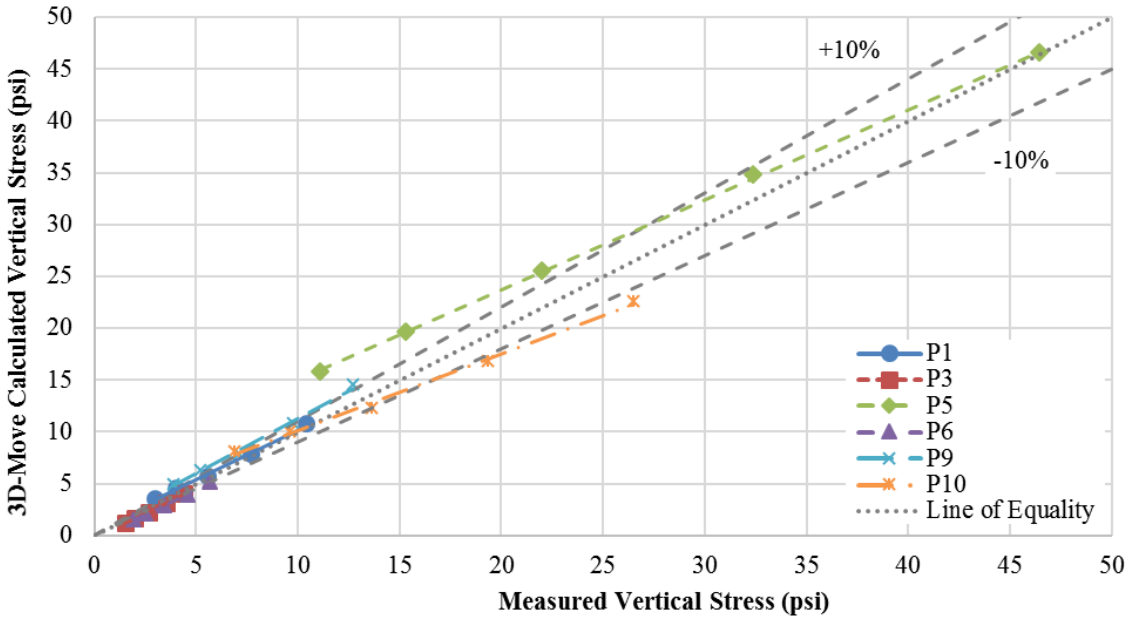

Figure 34. Graph. Comparison between 3D-Move-calculated versus measured σ_v in experiment No. 3.

Results of σ_{ij} at 5.91 inches below the SG surface were computed and converted to the corresponding triaxial testing conditions as outlined in section 3.4.1. Table 17 presents the result for the shear strength parameters estimation using the estimated σ_{df}. As before, by assuming an acceptable range for ϕ based on the identified soil classification, corresponding c values were estimated. The results of the ϕ and c can now be compared against the measured values for the SG material. As shown in table 17, a close match between measured and predicted soil strength parameters can be observed. These reasonable estimations of ϕ and c for totally different pavement structures and material properties can substantiate the validity and applicability of the proposed FWD-type methodology.

Table 17. Shear strength parameters estimation for SG materials used in experiment No. 3 and at LanammeUCR.

Experiment	Soil Classification	Typical Values of ϕ (Degrees)[19,20]	Estimated ϕ (Degrees)	Estimated c (psi)	Average of Estimated ϕ (Degrees)	Average of Estimated c (psi)	Measured ϕ (Degrees)	Measured c (psi)
Experiment No. 3	SC	32–42	32.0 34.0 36.0 38.0 40.0 42.0	3.8 3.4 3.0 2.5 2.1 1.6	37.0	2.7	38.0	2.0
LanammeUCR-AC2	High-plasticity silt	5–15	5.0 7.0 9.0 11.0 13.0 15.0	4.8 4.6 4.4 4.2 3.9 3.8	10.0	4.3	7.0	3.9
LanammeUCR-AC3	High-plasticity silt	5–15	5.0 7.0 9.0 11.0 13.0 15.0	4 3.8 3.6 3.4 3.2 3.1	10.0	3.5	7.0	3.9

As presented in table 14 through table 16, the load-induced σ_d at the highest load level is at least 40 percent of the estimated σ_{df}. Caution should be exercised when this value is much lower (below 30 percent) because the extrapolation of the hyperbolic relationship to near-failure condition may not provide proper estimates of σ_{df}. Under such circumstances, the FWD load level needed to induce an acceptable σ_d level in the SG layer can be estimated by extrapolating the data obtained at the lower load levels to reach the target percent of σ_{df}. Consequently, the FWD field testing and associated analysis should be repeated to include such load levels.

CHAPTER 4. SUMMARY AND CONCLUSION

The shear strength parameters of an SG layer are necessary inputs for assessing the risk of instantaneous shear failure under SHL movement of flexible pavements. These SG shear strength parameters are critical inputs for the stability analysis of a sloped pavement shoulder under an SHL movement. In this study, a novel methodology to estimate in-situ shear strength parameters of a pavement's SG layer based on nondestructive FWD testing undertaken at multiple load levels has been developed and verified.

In this methodology, σ_{ij} at a representative element in the SG is calculated first by using a layered LEP (e.g., 3D-Move Analysis software using static condition) to simulate each of the applied FWD load levels.[28] The analysis utilizes the backcalculated pavement layer moduli at each of the respective FWD load levels. Such an approach inherently takes into account the role of stress dependency in an unbound material. The implementation of backcalculated moduli in an LEP is a common practice in mechanistic–empirical pavement-design and -analysis procedures to obtain pavement responses. The calculated σ_{ij} is transformed to the equivalent stress conditions associated with triaxial compression tests (σ_d and σ_c) for each of the FWD load levels using the stress invariants (i.e., octahedral stress components). A hyperbolic relationship is subsequently fitted to the equivalent triaxial test datasets of σ_d and ε_1 to obtain the σ_{df}. The Mohr–Coulomb failure envelope equation is then used for estimating c of the SG by assuming an acceptable range for ϕ.

The validity of the proposed approach was explored using numerical simulations of FWD measurements and FWD data collected from large-scale experiments on full-scale pavement structures as well as APT facilities. A variety of unpaved and paved pavement structures was utilized in the verification process. It was found that the proposed FWD-based methodology is able to reasonably estimate the shear strength parameters of an SG layer with softening behavior. Such results were achieved when the highest induced σ_d levels in the SG layer under the FWD loading were in excess of approximately 30 percent of the σ_{df} obtained with the proposed approach. The hardening behavior for an SG material at the FWD state of stress indicated by a negative slope of ε_1/σ_d versus ε_1 is recognized as a limitation of the proposed approach.

REFERENCES

1. Hajj, E.Y., Siddharthan, R.V., Nabizadeh, H., Elfass, S., Nimeri, M., Kazemi, S.F., Batioja-Alvarez, D.D., and Piratheepan, M. (2018). *Analysis Procedures for Evaluating Superheavy Load Movement on Flexible Pavements, Volume I: Final Report*, Report No. FHWA-HRT-18-049, Federal Highway Administration, Washington, DC.

2. Nimeri, M., Nabizadeh, H., Hajj, E.Y., Siddharthan, R.V., Elfass, S., and Piratheepan, M. (2018). *Analysis Procedures for Evaluating Superheavy Load Movement on Flexible Pavements, Volume II: Appendix A, Experimental Program*, Report No. FHWA-HRT-18-050, Federal Highway Administration, Washington, DC.

3. Nimeri, M., Nabizadeh, H., Hajj, E.Y., Siddharthan, R.V., and Elfass, S. (2018). *Analysis Procedures for Evaluating Superheavy Load Movement on Flexible Pavements, Volume III: Appendix B, Superheavy Load Configurations and Nucleus of Analysis Vehicle*, Report No. FHWA-HRT-18-051, Federal Highway Administration, Washington, DC.

4. Nabizadeh, H., Hajj, E.Y., Siddharthan, R.V., and Elfass, S. (2018). *Analysis Procedures for Evaluating Superheavy Load Movement on Flexible Pavements, Volume IV: Appendix C, Material Characterization for Superheavy Load Movement Analysis*, Report No. FHWA-HRT-18-052, Federal Highway Administration, Washington, DC.

5. Nabizadeh, H., Nimeri, M., Hajj, E.Y., Siddharthan, R.V., Elfass, S., and Piratheepan, M. (2018). *Analysis Procedures for Evaluating Superheavy Load Movement on Flexible Pavements, Volume VI: Appendix E, Ultimate and Service Limit Analyses*, Report No. FHWA-HRT-18-054, Federal Highway Administration, Washington, DC.

6. Nabizadeh, H., Siddharthan, R.V., Elfass, S., and Hajj, E.Y. (2018). *Analysis Procedures for Evaluating Superheavy Load Movement on Flexible Pavements, Volume VII: Appendix F, Failure Analysis of Sloped Pavement Shoulders*, Report No. FHWA-HRT-18-055, Federal Highway Administration, Washington, DC.

7. Nabizadeh, H., Elfass, S., Hajj, E.Y., Siddharthan, R.V., Nimeri, M., and Piratheepan, M. (2018). *Analysis Procedures for Evaluating Superheavy Load Movement on Flexible Pavements, Volume VIII: Appendix G, Risk Analysis of Buried Utilities Under Superheavy Load Vehicle Movements*, Report No. FHWA-HRT-18-056, Federal Highway Administration, Washington, DC.

8. Batioja-Alvarez, D.D., Hajj, E.Y., and Siddharthan, R.V. (2018). *Analysis Procedures for Evaluating Superheavy Load Movement on Flexible Pavements, Volume IX: Appendix H, Analysis of Cost Allocation Associated With Pavement Damage Under a Superheavy Load Vehicle Movement*, Report No. FHWA-HRT-18-057, Federal Highway Administration, Washington, DC.

9. Kazemi, S.F., Nabizadeh, H., Nimeri, M., Batioja-Alvarez, D.D., Hajj, E.Y., Siddharthan, R.V., and Hand, A.J.T. (2018). *Analysis Procedures for Evaluating Superheavy Load Movement on Flexible Pavements, Volume X: Appendix I, Analysis Package for Superheavy Load Vehicle Movement on Flexible Pavement (SuperPACK)*, Report No. FHWA-HRT-18-058, Federal Highway Administration, Washington, DC.

10. Kondner, R.L. (1963). "Hyperbolic Stress-Strain Response: Cohesive Soils." *Journal of the Soil Mechanics and Foundations Division*, *89*(1), pp. 115–144, American Society of Civil Engineers, Reston, VA.

11. Duncan, J.M. and Chang, C.Y. (1970). "Nonlinear Analysis of Stress and Strain in Soils." *Journal of the Soil Mechanics and Foundations Division*, *96*(5), pp. 1,629–1,653, American Society of Civil Engineers, Reston, VA.

12. Von Quintus, H.L. and Simpson, A.L. (2002). *Back-Calculation of Layer Parameters for LTPP Test Sections, Volume II: Layered Elastic Analysis for Flexible and Rigid Pavements*, Report No. FHWA-RD-01-113, Federal Highway Administration, Washington, DC.

13. Schmertmann, J., Brown, P., and Hartman, J. (1978). "Improved Strain Influence Factor Diagrams." *Journal of Geotechnical Engineering*, *104*(8), pp. 1,131–1,135, American Society of Civil Engineers, Reston, VA.

14. National Cooperative Highway Research Program. (2004). *Guide for Mechanistic-Empirical Design of New and Rehabilitated Pavement Structures*, Transportation Research Board, Washington, DC.

15. Hajj, E.Y., Ulloa, A., Siddharthan, R., and Sebaaly, P.E. (2010). "Estimation of Stress Conditions for the Flow Number Simple Performance Test." *Transportation Research Record*, *2181*, pp. 67–78, Transportation Research Board, Washington, DC.

16. Nabizadeh, H., Hajj, E.Y., Siddharthan, R., Elfass, S., and Sebaaly, P.E. (2016). "Estimation of In Situ Shear Strength Parameters for Subgrade Layer Using Non-destructive Testing." *The Roles of Accelerated Pavement Testing in Pavement Sustainability*, pp. 525–538, Springer, Cham, Switzerland.

17. Nabizadeh, H., Hajj, E.Y., Siddharthan, R., Elfass, S., and Nimeri, N. (2017). "Application of Falling Weight Deflectometer for the Estimation of in-situ Shear Strength Parameters of Subgrade Layer." *Proceedings of the 10th International Conference on the Bearing Capacity of Roads, Railways and Airfields (BCRRA 2017), Athens, June 28–30, 2017*, pp. 743–749, Taylor & Francis Group, Abingdon, England.

18. Das, B.M. and Sobhan, K. (2014). *Principles of Geotechnical Engineering*, Cengage Learning, Stamford, CT.

19. Minnesota Department of Transportation. (2007). *MnDOT Pavement Design Manual*, MnDOT, Saint Paul, MN.

20. Koloski, J., Schwarz, S., and Tubbs, D. (1989). "Geotechnical Properties of Geologic Materials." *Engineering Geology in Washington*, *1*, Washington Division of Geology and Earth Resources, Bulletin 78. Available online: http://www.tubbs.com/geotech/geotech.htm, last accessed October 25, 2018.

21. Ostovar, M. (2016). *An Exploratory Experimental Evaluation of ε50 in c-ϕ Soils*, Master's thesis, University of Nevada, Reno, Reno, NV.

22. Federal Aviation Administration. "National Airport Pavement Test Facility Databases." Available online: http://www.airporttech.tc.faa.gov/Airport-Pavement/National-Airport-Pavement-Test-Facility-/NAPTF-Databases, last accessed September 19, 2017.

23. Raad, L. and Figueroa, J.L. (1980). "Load Response of Transportation Support Systems." *Journal of Transportation Engineering*, *106*(1), pp. 111–128, American Society of Civil Engineers, Reston, VA.

24. Glover, L.T. and Fernando, E.G. (1995). *Evaluation of Pavement Base and Subgrade Material Properties and Test Procedures*, Report No. FHWA/TX-96/1335-2-006, Texas Transportation Institute, College Station, TX.

25. Kim, Y.R. and Park, H. (2002). *Use of FWD Multi-Load Data for Pavement Strength Estimation*, Report No. FHWA/NC/2002-006, Federal Highway Administration, Washington, DC.

26. BAKFAA software V2.0. (2012). Backcalculation Software, Federal Aviation Administration, Washington, DC.

27. Rohde, G.T. and Scullion, T. (1990). *MODULUS 4.0: Expansion and Validation of the MODULUS Backcalculation System*, Report No. FHWA/TX-91/1123-3, Texas Transportation Institute, College Station, TX.

28. 3D-Move Analysis software V2.1. (2013). Developed by University of Nevada, Reno, NV. Available online: http://www.arc.unr.edu/Software.html#3DMove, last accessed September 19, 2017.

29. Garg, N. and Thomson, M.R. (1997). "Triaxial Characterization of Minnesota Road Research Project Granular Materials." *Transportation Research Record*, *1577*, pp. 27–36, Transportation Research Board, Washington, DC.

HRDI-20/01-19(WEB)E